INVOLVEMENT OF CEREBELLAR PURKINJE CELLS IN ADAPTIVE LOCOMOTION OF LARVAL ZEBRAFISH

DANIIL A. MARKOV

Dissertation zur Erlangung des akademischen Grades
des Doktors der Naturwissenschaften (Dr. rer. nat)

an der Fakultät für Biologie der
Ludwig-Maximilians-Universität München
München, den 26. November 2019

ERSTGUTACHTER
Prof. Dr. Herwig Baier

ZWEITGUTACHTER
Prof. Dr. Hans Straka

TAG DER ABGABE
26. November 2019

TAG DER MÜNDLICHEN PRÜFUNG
07. Juli 2020

Die Arbeit wurde am Max-Planck-Institut für Neurobiologie
in der Arbeitsgruppe von Dr. Ruben Portugues durchgeführt

Eidesstattliche Erklärung

Ich versichere hiermit an Eides statt, dass die vorgelegte Dissertation von mir selbständig und ohne unerlaubte Hilfe angefertigt ist.

München, 25. November 2019

Daniil Markov

Publication statement

The results presented in this PhD thesis are in preparation for submission to the *Nature Neuroscience* journal under the title *‘‘The cerebellum recalibrates a feedback controller involved in motor control’’*. Most of the figures were adapted from the manuscript, as were most of the Materials and methods and Results sections.

Acknowledgements

No words can express all the gratitude that I feel to those, who in one way or another shared my PhD path with me. I was very lucky to work with and receive support from a lot of truly amazing people, and without them, this work would not have been possible at all.

First off all, I would like to deeply thank my supervisor Ruben Portugues not only for giving me an opportunity to pursue my project in the incredible environment of the Portugues lab and for all the support he provided from the very beginning and through the entire project, but also for giving me complete freedom in my research. I hope that this helped me to develop essential skills required for being an independent scientist. Thank you Ruben for being an inexhaustible source of inspiration and motivation that you always shared with me and other lab members, showing us that at the end of the day, despite all the inevitably involved stress, science is fun. I wish everyone could have such a supervisor and friend.

I would like to sincerely thank all the members of the lab for having time to help, motivate, discuss and talk whenever needed, and most importantly, for creating an atmosphere of friendship that made the work much more enjoyable. Thank you Andreas for your unprecedented readiness to help in all aspects of life ranging from German paperwork to running imaging experiments. Your selfless generosity and responsiveness go way beyond the general line of duty. Furthermore, thank you for developing the gain drop paradigm and for generating the *PC*:epNtr-tagRFP transgenic line that made it all possible. Thank you Vilim for discussing the idea of the feedback control model, for showing me what a good programming practice means, and at the same time, for providing unlimited amounts of ice cream and pears to the lab. Thank you Luigi for helping me with everything, including the acquisition software and imaging experiment, while always staying in good mood; Hagar for staying late in the lab and running some evening fish for me; Elena for talking to me in every situation and listening to my career-related nagging; Tugce for her pilot experiments on the

lag paradigm and for the amazing baklava. Thank you Laura for the great scientific and emotional support and for being my personal example of an exceptional postdoc and a great person. Also special thanks to Andreas and Kata for translating the summary to German. One of my personal highlights during the PhD time was recording the *Little Fish* music video with Andreas, Patricia and my brother Mishka. Thank you so much for this unforgettable experience and fun. I am very grateful to all other current and former members of the lab with whom I was lucky to coincide in time and space: Virginia, Diego, You, Olga, Ot, and Joao, for being wonderful colleagues and friends.

I would like to thank the members of my Thesis Advisory Board: Ruben Portugues, Herwig Baier, Hans Straka, Hernán López-Schier and Ilona Grunwald Kadow, for being always supportive, constructive and critical during our meetings. I am convinced that without these meetings, this work would have been much worse and its author would have been much less happy.

I am very grateful to Michael Orger, Rita Felix, Hernán López-Schier and Gema Valera for being amazing collaborators. Trying to stimulate a single neuromast with Gema and not to drawn in tons of inferior olive responses with Rita will definitely remain in my memory for the entire life.

This work would obviously not have been possible without healthy zebrafish. I would therefore like to thank Krasimir, Karin and all the fish caretakers for keeping the fish facility and its habitants in perfect shape and for helping me with any fish-related issues and questions.

My research as well as my everyday life in Germany would have been much more difficult without the helpful administration of MPIN. Thank you Anne, Sabine, Gabi, Melanie, Patricia, Stefanie (and all the other wonderful people as well) for being such a great help throughout the last years.

During my PhD, I was very lucky to be a part of the International Max Planck Research School for Life Sciences. Thank you Hans-Jörg, Ingrid, Maxi, Marta, Amy and Viktoria for supporting me, coordinating the IMPRS-LS program, ensuring that my TAC meetings happen on time, and organizing multiple wonderful workshops and other events.

Outside the institute, I would like to thank all my friends in Munich for making my life truly full and bright. Jan, Susy and Gabe for playing Irish music with me, Serj for constant challenging to be as good as him, Natasha, Pasha and Lena for wonderful dinners and stress-free conversations about life.

I would definitely not be at this point in my life without my wonderful family. My mom and dad were the ones who infected me with interest in nature, and no words can express my gratitude for their love, support and faith in me through my entire life. The same applies to my amazing brothers. Thank you Alex for being the most cheerful and merry person I ever knew. Thank you Mishka for always being so kind despite my frequent misbehavior and for the ability to generate elegant programming algorithms on the fly during our phone calls whenever needed.

Finally, it is impossible to properly express all my gratitude to my dear wife and friend Arina. Thank you so much for selflessly giving me freedom and possibility to work hard on my research while keeping our family together. Thank you so much for believing in me even at times when I did not.

Summary

Animals need to adapt their behavior to survive and be successful in a constantly changing environment. Behavioral adaptations can be evoked by two mechanisms: feedback control and internal models. A feedback controller compares current sensory state with desired state and generates a motor output that minimizes their difference; such simple controllers can produce adaptive behavior without changing their own intrinsic parameters. In the central nervous system, however, feedback control is limited by long temporal delays associated with sensory processing required to estimate current sensory state. To overcome this limitation, internal models learn previous sensory-motor history to update parameters of motor control in a predictive manner. In the present study, I use multiple perturbations in visual feedback to show that larval zebrafish acutely adapt their swimming behavior to these perturbations. These acute behavioral changes do not affect an initial stereotyped ballistic portion of the swimming bouts that lasts ~ 220 ms and are unaffected by a pharmaco-genetic ablation of Purkinje cells – the major locus of internal models, suggesting that acute adaptation results from a feedback control mechanism. I support this hypothesis by modelling a simple feedback controller that is based on temporal integration of sensory evidence. The controller is able to closely reproduce all observed aspects of acute adaptation. The main assumption of the model: existence of temporal sensory integration in the larval zebrafish brain is supported by whole-brain functional imaging. On the other hand, during long-term adaptation, larval zebrafish gradually change their behavior, including their swimming kinematics during the ballistic period. In contrast with the acute short-term changes, these behavioral alterations are cerebellum-dependent. In conclusion, adaptive locomotion in larval zebrafish should be understood as a feedback control system whose intrinsic parameters can be modified by cerebellar output.

Zusammenfassung

Tiere müssen ihr Verhalten anpassen, um in einem sich verändernden Lebensraum zu überleben. Diese Anpassungen im Verhalten können durch zwei Mechanismen hervorgerufen werden: Rückkopplung und interne Modelle. Ein Regelkreis basierend auf sensorischer Rückkopplung vergleicht den Ist-Zustand mit dem Soll-Zustand und generiert dementsprechend ein Motorsignal, das die Differenz der Zustände minimiert. Solche einfachen Regler können ohne die Veränderung von internen Parametern adaptives Verhalten hervorrufen. Im zentralen Nervensystem sind jedoch diese Regelkreise limitiert durch lange zeitliche Verzögerungen aufgrund der Berechnung des sensorischen Ist-Zustandes. Um diese Einschränkungen zu umgehen, können interne Modelle verwendet werden, die mit Hilfe vorangegangener sensomotorischer Übersetzungen Motorparameter vorhersagen. In dieser Studie verwende ich mehrere Veränderungen in der visuellen Rückkopplung, um zu zeigen, dass Zebrafischlarven ihr Schwimmverhalten aufgrund dieser Veränderungen akut anpassen. Diese akuten Anpassungen im Verhalten beeinflussen allerdings nicht die stereotypen, ballistischen Eigenschaften einzelner Schwimm-Ereignisse („bouts“), die ca. 220 ms andauern. Des Weiteren sind diese beeinträchtigt durch pharmakologisch-genetische Ablationen von Purkinje-Zellen, welche einen Hauptort interner Modelle bilden, was darauf hinweist, dass akute Anpassungen von klassischen Rückkopplungsmechanismen gesteuert werden. Zur Unterstützung dieser Hypothese stelle ich ein Modell eines einfachen Rückkopplungsreglers vor, welches auf der zeitlichen Integration sensorischer Informationen basiert. Dieses Modell kann fast alle beobachteten Aspekte akuter Verhaltensanpassung reproduzieren. Die Hauptannahme des Modells, dass eine zeitliche Integration sensorischer Information im Gehirn von Zebrafischlarven existiert, wird durch funktionelle Bildgebung des gesamten Gehirns unterstützt. Dem gegenüber steht, dass Zebrafischlarven ihr Verhalten während einer Langzeitadaptionsstudie, inklusive der Kinematik ihres Schwimmverhaltens,

graduell anpassen. Im Kontrast zu akuten Verhaltensanpassungen sind diese Verhaltensänderungen abhängig vom Kleinhirn. Zusammenfassend kann adaptives Verhalten während der Fortbewegung in Zebrafischlarven als Rückkopplungssystem verstanden werden, dessen intrinsische Parameter durch Signale des Kleinhirns modifiziert werden.

Table of Contents

Eidesstattliche Erklärung iv

Publication statement v

Acknowledgements vi

Summary x

Zusammenfassung xi

1. Introduction 1

1.1 Adaptive control and internal models 1

1.2 Cerebellum as a neuronal substrate of internal models 10

1.3 Larval zebrafish as a model organism to study adaptive behavior 19

1.4 Thesis objectives 23

2. Materials and methods 24

2.1 Model organism and subject details 24

2.2 Closed-loop experimental assay in head-restrained preparations 29

2.3 Behavioral experiments 35

2.4 Modelling a feedback controller of acute adaptation 38

2.5 Functional imaging experiments 42

3. Results 48

3.1 Acute OMR adaptation to changes in visual reafference 48

3.2 Involvement of PCs in acute OMR adaptation 56

3.3 Feedback control model of acute OMR adaptation 60

3.4 Long-term OMR adaptation 68

3.5 Involvement of PCs in long-term OMR adaptation... 71

4. Discussion... 73

4.1 Feedback control mechanism of acute OMR adaptation 73

4.2 Long-term cerebellar effects on the feedback controller................................. 75

4.3 Concluding remarks, limitations and future directions 77

5. Appendix 82

5.1 List of abbreviations 82

5.2 List of tables and figures.. 83

5.3 MATLAB code of the feedback control model of acute adaptation............... 84

Bibliography 90

Declaration of contributions 96

List of publications.. 97

Curriculum vitae 98

1. Introduction

1.1 Adaptive control and internal models

All living organisms have to survive and be successful despite ever-changing conditions of their environment. If the environment were an unchanging entity, e.g. the temperature, pressure, humidity, wind conditions etc. were always the same, the food and mating partners were always around at the same place, then executing the same actions over and over again might have resulted in reaching the goals successfully. However, we can leave this fantasy world to science fiction writers and postulate that in our world, conditions constantly change, and organisms have to adapt to these changes. The means to achieve this universal goal of adaptation to the environment can be observed on different organizational levels: from molecular to behavioral. For example, in some prokaryotic organisms such as *E. coli*, the molecular machinery of their flagella is organized in such a way that enables the bacteria to modulate the rotation of the flagella to reach an attractive chemical during chemotaxis (Turner et al., 2000; Yuan et al., 2010). As a result, a bacterium will reach the attractant regardless to where it is located with respect to the bacterium, i.e. under different environmental conditions.

In animals, the highly complex nervous system has evolved not only to coordinate activity of different parts and systems of the body, but also to ensure that behavior is adequate to the environmental conditions, in a sense that animals should be able to reach a desired goal under different conditions and within different contexts. This must involve modifying the behavioral output when the conditions change, a process referred to as behavioral adaptation. This section describes two possible mechanisms that can underlie adaptive behavior: feedback control and internal models.

1.1.1 Feedback control

The easiest way to produce adaptive behavior under different and often unpredictable external conditions is to constantly monitor the current sensory state of the body and to produce behavior that brings it closer to the desired state. Such behavior can be generated by a closed-loop negative feedback controller (or, simply, a feedback controller, Figure 1.1). To illustrate how a typical feedback controller works, let us consider a simple control system, such as a thermostat, that tries to maintain a desired internal temperature despite inconstant external temperature. Let us assume, for simplicity, that the thermostat is instrumented only with a heating element because the external temperature is expected to always be lower than the desired temperature so that no active cooling is required to maintain the desired temperature. The feedback controller “knows” the desired temperature, compares it with the current internal temperature measured by a sensor (feedback signal), and sends a motor command to the heating element if the current temperature is less than desired (i.e. if there is a sensory error). Such control system will maintain the desired temperature under different environmental conditions, i.e. produce adaptive behavior.

Thanks to their ability to reach the same goal under different conditions, feedback controllers are widely used in engineering. In the central nervous system (CNS), however, feedback-based mechanisms of motor control are limited by at least three factors.

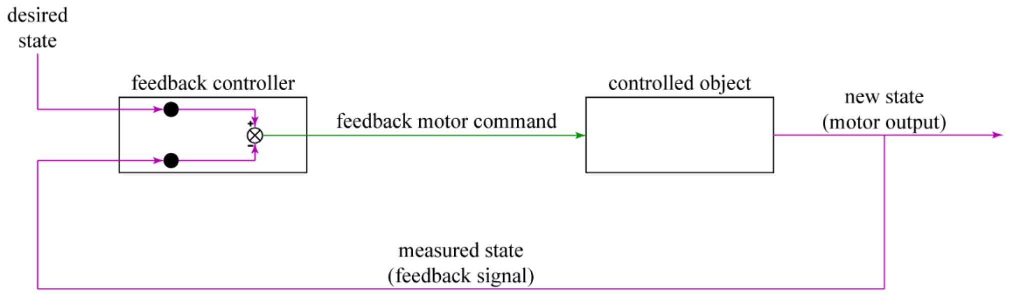

Figure 1.1. Feedback controller

A feedback controller computes the difference between the desired state (set in the controller) and the current state (measured by a sensor), and sends a motor command to the controlled object (e.g. a heating element of a thermostat). If the resulting action brings the current state closer to the desired state, such control system will maintain the desired state under different environmental conditions, i.e. produce adaptive behavior. Magenta color represents variables expressed in sensory coordinates (e.g. temperature) and green color represents variables expressed in motor coordinates (e.g. voltage). This color-code is used throughout the thesis. Essentially, any controller performs sensory-motor transformation (magenta to green), whereas any controlled object performs an inverse process, i.e. transforms a motor command into some sensory consequences (green to magenta).

The first, most important limitation is associated with long temporal delays involved in processing of sensory information, which is required to measure current sensory state. Whilst in engineered control systems feedback loops can be made fast, the CNS requires a substantial amount of time to detect and process sensory feedback and react accordingly. These time delays vary across sensory modalities. Thus, estimates of the delay involved in using visual feedback vary from about 100 to 300 ms (Barnett-Cowan and Harris, 2009; Brenner and Smeets, 2003; Desmurget and Grafton, 2000; Saunders and Knill, 2003; Saunders and Knill, 2005), whereas processing delays of proprioceptive information are estimated as 40 – 150 ms (Flanders and Cordo, 1989; Flanders et al., 1986; Starr et al., 1981). If the processing of sensory information is long with respect to the duration of the motor action, the current sensory state will change dramatically by the time the feedback signal starts to influence the motor command, thus implementing an inappropriate correction based on out-of-date information. It is well known in engineering that feedback control with time-delayed inputs often produces oscillatory behavior (Kakei et al., 2019). This can be nicely illustrated by a simple everyday-life example (modified from Shadmehr et al., 2010). Let us consider a person who aims to take a shower in an unfamiliar bathroom using pure feedback-based mechanism to control the water temperature. Assuming that the original position of the temperature control knob corresponds to the minimal water temperature, the water will be too cold when the person initially turns it on. Naturally, the person will then aim to heat the water by adjusting the knob until it reaches the person's favorite temperature. Since the delay between adjusting the knob and feeling the effects of this adjustment is notoriously long, the person will continue turning up the heat so that by the time the water finally reaches the favorite temperature, the heat adjustment will already be at a higher level. Then, when the water becomes too hot, the person will adjust the control knob to cool down the water. However, thanks to the response delay, the temperature will continue to rise for some time. The person will responds by turning down the temperature control even farther, and when the temperature finally responds, the poor person is soon freezing, and the cycle repeats. Thus, using feedback-based control mechanisms with long time delays results in an alternating scalding and freezing experience.

The second limiting factor is that any physiological sensor inevitably has some inaccuracies, compound by neural noise, that lead to errors in the measurements making feedback detection less accurate.

Finally, the parameters that the CNS might aim to control, such as joint angle or angular velocity, often cannot be measured directly due to lack of respective sensors (Miall et al., 2007). Thus, to estimate current joint angle, the CNS must decode it from indirect information provided by muscle spindles.

1.1.2 Internal models

To overcome the aforementioned limitations of feedback control and yield accurate adaptive behavior, the CNS must utilize some kind of predictive mechanisms. This becomes especially important when motor control has to be performed rapidly, as in capturing a fast and evading prey or fast reaching arm movement towards a target. Essentially, the process of prediction is inextricably linked to the process of modelling because in order to predict something, one must have some understanding of the rules underlying the process, i.e. have a model of this process. It was therefore proposed that the CNS contains, in one form or another, internal models of the motor apparatus (Kawato, 1990; Kawato et al., 1987; Wolpert et al., 1995). The essence of internal models is that they monitor inputs and outputs of a controlled system and eventually learn a transfer function of this system. Depending on whether internal models learn a forward or an inverse function, they can be categorized into two groups: forward models and inverse models. Forward models are able to predict sensory consequences of a motor command and can be therefore used as predictors (Flanagan and Wing, 1997; Flanagan et al., 2003; Shadmehr et al., 2010; Wolpert et al., 1995). In case of a thermostat, a trained forward model might predict, for example, that sending a certain voltage to a heating element will result in increasing the temperature by a certain value or at a certain speed, and this prediction will be available for the controller long time before the delayed feedback signal arrives. In turn, inverse models predict a motor command that is required to achieve desired sensory consequences and can be therefore used as feedforward controllers (Kawato, 1999; Kawato and Gomi, 1992b; Sabes, 2000; Shidara et al., 1993; Wolpert et al., 1998). Thus, an inverse model might predict that in order to increase the temperature by a certain value or at a certain speed, a certain voltage must be sent to a heating element.

If we develop the aforementioned example of a naïve person trying to take a shower in an unfamiliar bathroom, one could say that after several scalding-freezing cycles caused by delayed feedback, the person will understand how the temperature control knob works, i.e. acquire an internal model of the knob. This prior knowledge, the internal model, can be used instead of (or in addition to) a feedback control mechanism. In this example, the person might acquire a forward model that encapsulates the idea that a certain position of the knob results in a certain water temperature. Instead of comparing her favorite temperature with the delayed feedback, the person might compare it with the feedback *predicted* by the forward model and adjust the knob until this prediction matches the goal. Alternatively, the person might acquire an inverse model and perform a feedforward adjustment of the knob to the position that she predicts to result in her favorite water temperature.

Both forward and inverse internal models can be used to solve a variety of motor control problems, and their exact roles are largely determined by their placement within a control system. Two examples of such placements are demonstrated in Figure 1.2.

In Figure 1.2a, a copy of the motor command generated by a feedback controller (efference copy) is sent to a forward model of the controlled object. The model learns a forward transfer function of the object, i.e. what sensory feedback follows different motor commands. Therefore, sensory feedback acts as a teaching signal that trains the forward model (indicated by a wavy line). A trained model is able to predict consequences of the current motor command. The generation of the prediction is fast because it does not depend on slow sensory processing and a feedback controller can use this prediction instead of the measured feedback signal. In this example, output of a forward model *substitutes* for measured sensory feedback, however it is important to note that prediction of a forward model can also *supplement* measured sensory state. The CNS might combine forward modelling with sensory observations in order to produce more accurate state estimation than can be achieved using either of these mechanisms on their own in a way similar to Kalman filtering (Miall et al., 2007; Wolpert et al., 1995).

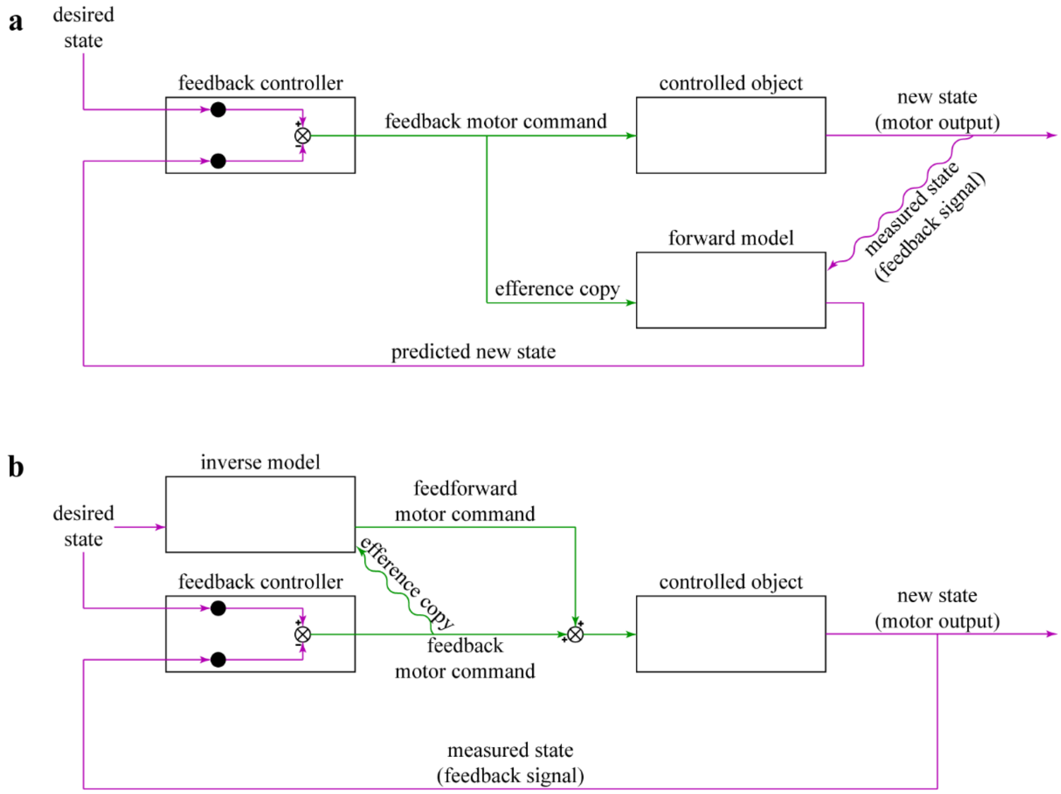
a
desired state
feedback controller
feedback motor command
controlled object
new state (motor output)
measured state (feedback signal)
forward model
efference copy
predicted new state
b
inverse model
desired state
feedforward motor command
efference copy
feedback controller
controlled object
new state (motor output)
feedback motor command
measured state (feedback signal)

Figure 1.2. Possible placements of internal models within a feedback control system

a. A feedback control system with a forward model. **b**. A feedback control system with an inverse model (feedback-error-learning model [Kawato, 1990]). Wavy lines denote the teaching signals used by internal models to learn the transfer function. Note that the teaching signal is expressed in the same coordinates as the output of an internal model (sensory for the forward model and motor for the inverse model). See details in the text below. *Panel **b** is adapted from Kawato and Gomi (1992a), with permission.*

Inverse functions are often less intuitive than forward functions, and placement an inverse internal model into a control system in a reasonable way seems to be a more difficult task. A possible way to incorporate an inverse model into a feedback control system was proposed by Mitsuo Kawato (1990) and was termed a feedback-error-learning scheme (Figure 1.2). In this scheme, the final motor command that is fed to the controlled object is a linear sum of a feedback motor command produced by a feedback controller and a feedforward motor command produced by an inverse model. The inverse model monitors the relationship between the desired sensory state and a feedback motor command, and learns to produce a feedforward motor command that minimizes the feedback command. In this case, the teaching signal is a feedback motor command (indicated by a wavy line), which is only generated by the feedback controller if measured sensory feedback differs from the desired sensory state, i.e. if there is a sensory error (see Introduction section 1.1.1). Therefore, by learning to minimize the feedback motor command, an inverse model learns to minimize the sensory error, which is highlighted in the title of this scheme: feedback-error-learning. Eventually, a trained inverse model produces a good feedforward control, “good” in a sense that it leads to the desired sensory state and does not depend on long-delayed sensory feedback (Kawato, 1990; Kawato and Gomi, 1992a; Kawato and Gomi, 1992b).

Originally emerged as a theoretical concept, the hypothesis that internal models exist in the CNS is nowadays supported by a significant body of experimental evidence, some of which is outlined below.

One line of evidence comes from human psychophysical studies of grip force coordination during arm movements with hand-held objects (Flanagan and Tresilian, 1994; Flanagan and Wing, 1990; 1993; 1997; Flanagan et al., 1993). In these studies, subjects were asked to perform different movements with an arm while holding an object with the tips of the thumb and index finger. Acceleration during arm movements induces inertial load forces applied to the hand-held object. In one study (Flanagan and Wing, 1997), other types of load forces (viscous and elastic loads) were artificially applied by force-served linear motors attached to the manipulandum that the subjects were holding and moving. Either way, fluctuations in load force require adjustments of the grip force with which the object is held to prevent its slipping. These studies demonstrated that the grip force is modulated in parallel and thus anticipates the load force, indicating that the CNS can predict the load force to adjust the grip force and prevent slipping of the held object. Since the load force depends on both the load properties and the kinematics of the moving arm, this result indicates that the CNS has an internal model of the object dynamics (e.g., how heavy the object is predicted to be) and of the loaded moving arm (e.g., by how much the load force is predicted to change during a given arm acceleration).

Another example supporting existence of internal models in the CNS of a different model system is evident in prey interception behavior in dragonflies (Mischiati et al., 2015). In this study, careful analysis of dragonfly’s head and body orientation and position has detailed the strategy used by dragonflies during prey interception. This strategy includes predictive rotations of the head to continuously track the moving target and using these rotations to align the body orientation with the prey’s path while remaining directly below the prey and closing the vertical distance. These steps must rely on internal models of both body dynamics and moving target. For example, predictive head rotations nullify the prey-image drift that could be caused by both own body movements and prey motion, implying internal models that can predict image drift from motor commands sent to the wings and from the target motion at a constant velocity.

As the matter of fact, the question of whether internal models exist in the CNS can be viewed as a question of terminology rather than biology. If we accept that the CNS uses predictions for accurate motor control and that these predictions are provided by something termed internal models, we logically conclude that internal models exist. In his review about internal models of eye movements, Stephen Lisberger (2009), wrote, “the question is not whether the brain operates as an internal model of the body. It must. Instead, the questions are whether internal models are localized at specific sites in the brain, how they are constructed through neural circuits, and whether specific patterns of neural discharge can be understood in terms of internal models."

1.2 Cerebellum as a neuronal substrate of internal models

It is widely believed that one of the major neuronal sites of internal models in vertebrates is the cerebellum. This section describes the basic circuit architecture of this brain structure, discusses why this architecture is perfectly suited for acquiring and storing internal models, and provides direct experimental evidence of internal models in the cerebellum.

1.2.1 Architecture of the cerebellum

The cerebellum has attracted interest of both theoretical and experimental biologists for a long time due to its well-documented microanatomy combined with its prominent involvement in motor control. The roots of our present knowledge on cerebellar organization were provided by the famous anatomical studies of Ramón y Cajal in the 19th century. Cerebellar architecture has several characteristic features some of which were captured by Cajal using silver staining method whereas the others were discovered later thanks to the advent of new techniques (Sotelo, 2008).

On the macroanatomical level, the cerebellum can be divided into 3 functional and anatomical parts based on their afferent connections and phylogenetical age (Dow, 1942). The most ancient part, the vestibulocerebellum, is already present in cyclostomes and interacts with vestibular and oculomotor systems. The spinocerebellum first appears in fish and is innervated mainly from the spinal cord. The phylogenetically youngest part, the cerebrocerebellum, receives projections from the cerebral cortex with switching in the pontine nuclei.

In most vertebrates, the cerebellum is composed of stratified cerebellar cortex surrounding the white matter, in which lie the deep cerebellar nuclei (DCN). The cerebellar cortex contains two main cell types that play the dominant role in the cerebellar circuit (Figure 1.3): Purkinje cells (PCs) and granule cells (GCs), as well as different types of interneurons. PCs are GABAergic neurons and their morphology is characterized by a large, nearly two-dimensional, and elaborate dendritic arbor oriented orthogonally to the longitudinal axis of the cerebellar cortex. PCs receive two main inputs: parallel fiber (PF) input and climbing fiber (CF) input.

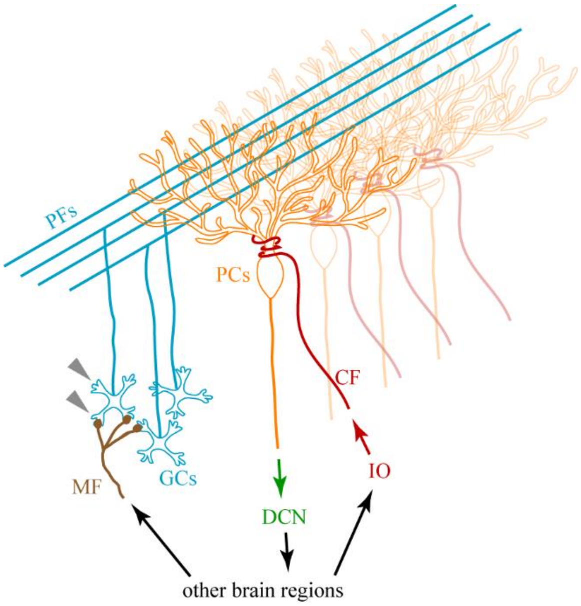

Figure 1.3. Main connections of the olivo-cerebellar system

PCs – Purkinje cells, GCs – granule cells, PFs – parallel fibers, MF – mossy fiber, CF – climbing fiber, IO – inferior olive, DCN – deep cerebellar nuclei. Gray triangles indicate dendritic claws of GCs. See details in the text of this section.

PFs are the axons of GCs that span through the cerebellar cortex perpendicularly to the PCs' dendritic trees, with each PF making contacts with multiple PCs' along the way. GCs are small glutamatergic neurons that typically have four dendrites, each terminating with a peculiar structure called dendritic claw (indicated with gray triangles on Figure 1.3). GCs are the most numerous cell type in the CNS, their number in human cerebellum is estimated as 50 billion (Llinás et al., 2004), constituting more than a half of the total neuron count in the human brain. Thanks to their large and highly arborized dendritic trees, each PC receives inputs from about 200'000 PFs, more than any other cell type in the brain (Llinás et al., 2004). Such unprecedented high number of GCs and level of PF inputs convergence are among the most peculiar features of the cerebellar architecture. GCs receive their main inputs from mossy fibers (MFs) that provide the cerebellar cortex with motor-related and sensory information of different modalities from multiple brain regions including cerebral cortex, vestibular nuclei, reticular formation, pontine nuclei, spinal cord, superior colliculi, locus coeruleus and red nucleus (Purves et al., 2004). In addition to innervating the GCs, MFs send collaterals to the DCN (Shinoda et al., 1992) (these collaterals are not shown in Figure 1.3 for simplicity).

The second main input to PCs, the CFs, is in every way different from the MF - PF input. It originates in a single brainstem nucleus, the inferior olivary nucleus (or, simply, inferior olive, IO). Functionally and anatomically, the IO is inextricably linked with the cerebellum, so they are often collectively called the olivo-cerebellar system. An IO axon branches into about 10 CFs, each innervating the cell body and proximal dendrites of a single PC, and each PC receives input from only one CF. However, a single CF forms about 300 synaptic connections with its target PC (Llinás et al., 2004). As a result, a single action potential in a CF induces a powerful activation event in the PC, termed the complex spike (Eccles et al., 1966). Additionally, olivocerebellar axons send collaterals to the DCN and lateral vestibular nucleus, which is very similar to the DCN by the nature of its afferent and efferent connections (these collaterals are not shown in Figure 1.3 for simplicity). IO receives afferent inputs from the spinal cord, multiple brain stem regions including the red nucleus, cerebral cortex, and from small inhibitory neurons of the DCN. Thus, the inhibitory feedback regulation of this important afferent input of the cerebellum is carried out.

Efferent output from the cerebellar cortex is formed solely by the axons of PCs. These axons terminate on DCN neurons that, in turn, send their projections outside the cerebellum and innervate multiple brain regions including pons, vestibular nuclei, spinal cord, ventral thalamic nuclei, red nucleus, and reticular formation. Additionally, a distinct subpopulation of DCN neurons – small GABAergic neurons – project to the IO (de Zeeuw et al., 1989; Fredette and Mugnaini, 1991). Therefore, output from the cerebellum is formed by axons of DCN neurons, with an exception of a group of PCs projecting to the lateral vestibular nucleus directly without switching in the DCN.

1.2.2 Internal models in the cerebellum

Another very interesting feature of the cerebellum is that it is extremely well conserved throughout evolution (Llinás et al., 2004). The main cerebellar cell types, their morphology and connections described above are markedly similar in fish, birds and mammals (insignificant differences of the fish cerebellum are mentioned in Introduction section 1.3.1). In addition, this architecture is similar across subdivisions of the cerebellum regardless of which parts of the brain they interact with. Indeed, the circuitry of the cerebellar cortex described above is the same in the vestibulocerebellum, spinocerebellum and cerebrocerebellum. Together with the fact that the cerebellum contains more than a half of the total number of neurons in the CNS, this indicates that this brain structure carries out a very important function. Apparently, the circuit that first appeared in cyclostomes in the form of the vestibulocerebellum was preforming some computation that appeared to be very advantageous, so that during evolution, the very same mechanism has extended to interact with many other brain regions involved in functions far beyond vestibuloocular control.

Perhaps, one of the most accepted hypothesis of what could be the general function of the cerebellum is that the cerebellum acts as a neuronal substrate for some kind of internal models (for reviews, see, for example, Lisberger, 2009; Nowak et al., 2007; Wolpert et al., 1998). Theoretical considerations demonstrating that the cerebellar circuitry is perfectly suited for storing and acquiring internal models, as well as some loss-of-function experiments directly supporting this hypothesis are presented in the next paragraphs.

Any kind of internal model, no matter what process it is trying to predict, should have access to sensory information of different modalities as well as to efferent copies of motor commands, in order to learn relationships between them (a transfer function). As mentioned above, the cerebellum receives inputs from a variety of brain regions and therefore has a perfect location within the brain to satisfy this condition.

The second crucial feature of internal models is their flexible nature, their ability to learn and update transfer function based on received afferent inputs. According to the theory of cerebellar function proposed by David Marr (1969) and James Albus (1971), the cerebellum can form associative memories between particular patterns of PF inputs and PCs' outputs. The Marr-Albus model was based on three central ideas. 1) PF input carries contextual sensory-motor information from the body and environment. 2) CF input carries some form of error signal that informs the cerebellar cortex if the current movement pattern does not reach the desired goal and therefore needs to be updated. 3) CF input can modify synaptic weights of currently active PF-PC synapses. A decade later, using electrophysiological recordings from cerebella of decerebrated rabbits, Ito et al. (1982) has demonstrated that simultaneous stimulation of MF and CF lead to long-term depression of PF-PC synapses involved in this conjunctive stimulation. Subsequently, other forms of synaptic plasticity at multiple sites of the cerebellum have been discovered (for a review, see

Tabata and Kano, 2009). Cerebellar plasticity indicates that the cerebellum satisfies the second criteria of internal models: ability to learn.

Finally, such a high number of GCs and PF inputs to a given PC can also make sense in the context of internal models. In behaving animals, a good control system must produce accurate and fast movements under a nearly infinite amount of possible environmental conditions while the motor commands required to reach a desired goal depend on these conditions. For example, from the point of view of required motor control, lifting an arm by 10 cm while standing on both feet is a very different task from lifting an arm by 10 cm while standing on one foot. Or lifting an empty arm versus a loaded arm. Or lifting an arm after exhaustive exercising versus after rest. In all cases, the pattern of muscle activation, and thus the motor control, must be different depending on the context. High number of GCs and high number of PF inputs to a given PC may ensure that any possible context can be represented by at least one pattern of PF-PC synapses. Additionally, generation of cerebellar long-term depression only at currently active PF-PC synapses may ensure that only the internal model that is important under these particular contextual conditions is a subject to change. These ideas formed the basis of the hypothesis that the cerebellum contains multiple modules of internal models (Wolpert and Kawato, 1998). The hypothesis postulates that each small module receives its own unique combination of inputs and is responsible for controlling a small parameter (or set of parameters) of the body movements (e.g., one joint angle or length of one group of muscles). According to this hypothesis, if the motor action needs to be improved, only those internal models are updated, that are engaged in ongoing movement, and only those *inputs* of these models, that represent current context. This can explain, why learning a new arm movement in one context (e.g. learning how to play a guitar) does not affect previously learned arm movements in other contexts (e.g. playing a piano), or why learning an arm movement does not affect previously learned leg movements. Modular organization of internal models within the cerebellum was supported by fMRI studies in humans (Imamizu et al., 2000; 2003).

Perhaps, the most direct way to prove that a given brain structure is involved in a particular function is manipulating the activity of this structure (as an option, destroying this structure) and monitoring the resulting change in its putative function. Destruction of the cerebellum does not produce paralysis indicating that to a certain extent, motor control can be carried out without the cerebellum. However, cerebellar patients often generate inaccurate and uncoordinated behavior, suggesting that the cerebellum is required to correct and improve motor control, as well as to place motor sequences in the context of the total sensory-motor state. One of the most common cerebellar symptoms is intention tremor – oscillation of the patient's limbs during goal-directed movements. This oscillation is markedly similar to oscillation of a feedback control system with long sensory delays (see Introduction section 1.1.1) and can therefore be understood as impaired motor performance when control relies solely on sensory feedback after the internal models are destroyed.

If sensory feedback arrives at a controller after a substantial temporal delay, the controller would estimate the current state of the system based on out-of-date information, thus the estimated state would lag behind the real state. In one loss-of-function study (Miall et al., 2007), the authors tested whether cerebellum is involved in accurate state estimation. To this end, they developed an arm-reaching task, in which the performance depended on how correctly the subjects estimated the position of the hand before the reaching movement. The subjects were instructed to slowly move their right index finger to the right or left (slow preparation movement), and then, after they hear an auditory go-cue, to rapidly move the finger in order to reach a target displayed on the screen (fast reaching movement). Since the reaching movements were fast, they could not be efficiently corrected online using sensory feedback after their initiation. As a result, trajectories of the reaching movements, at least to some extent, had to be planned in advance during the latency period between the go-cue and initiation of the movement, and the performance depended on accurate estimation of the hand position during this period. In some trials, the activity of the lateral cerebellum was perturbed during this period using transcranial magnetic stimulation (TMS), and performance errors of these trials were higher than during non-TMS trials. Importantly, the direction of the TMS-induced errors was the same as the direction of the slow preparation movement: e.g., if a subject was slowly moving hand to the right before the go-cue, the reach-to-target movement was biased towards the right. This result can be interpreted if we assume that the estimation of the hand position results from two cooperating mechanisms: one based on sensory feedback from the arm, and the other based on a cerebellar forward model. Position estimation during TMS trials was forced to rely solely on slow sensory feedback and therefore lagged behind the real position. As a result, when the slow preparation movement was to the right, TMS stimulation resulted in estimating the hand position as being more to the left than it really was, and the reaching trajectory was biased to the right, thus increased performance error. This interpretation is further supported by the fact that TMS stimulation did not increase the performance error if the initial hand position before the go-cue was static, i.e. if there was no preparation movement. Indeed, in this case, the position of the hand can be accurately estimated only from sensory feedback, as there were no dynamical changes in the hand position to be modelled. In addition, the magnitude of TMS-induced errors and hand velocity during the preparation movements suggested that reach-to-target movement during TMS-trials was planned based on the hand’s position 138 ms before the real position, consistent with reported proprioceptive feedback delays (Flanders and Cordo, 1989; Flanders et al., 1986; Starr et al., 1981).

In a different study (Izawa et al., 2012), the authors also asked whether cerebellum functions as a forward model that predicts sensory consequences of motor actions. Cerebellar patients and healthy control subjects were holding a robotic arm and performed rapid shooting movements towards a target displayed on a screen. After each movement, the robotic arm brought the hand back to the central starting position. Direct view of the hand was blocked from the subjects; however, a cursor representing its position was also displayed on the screen in most trials. The experimental paradigm included pre-adaptation, adaptation and post-adaptation phases. The pre- and post-adaptation trials included the so-called localization trials, during which no target or cursor representing the hand position were displayed. The subjects were asked to perform untargeted shooting arm movements and to report where they think their hand crossed the circle presented on the screen, i.e. the final angular position of the hand. Performance during localization trials depends on how well subjects can estimate the movement trajectory based on motor command without any visual feedback. Therefore, this performance can be interpreted as a readout of the forward model output. During the adaptation phase, the angle between actual arm movements and the cursor movement was gradually increased from trial to trial, so that the subjects needed to recalibrate their motor commands to ensure that the cursor still reaches the target. Both cerebellar patients and healthy control subjects demonstrated similar performance during the adaptation phase, indicating that a healthy cerebellum is not required for modifying the motor command if sensory feedback of these commands changes. Moreover, performance during the pre-adaptation localization trials was also indistinguishable between the groups, indicating that before the adaptation both cerebellar patients and healthy controls could correctly predict the movement trajectory from the motor command. However, performance during the post-adaptation localization trials was different between the groups. Healthy subjects' reported angular position of the hand after shooting movements was shifted with respect to the real hand position by the angle that the subjects learned to compensate during the adaptation. This indicates that changing the relationship between motor action and its sensory feedback leads not only to behavioral adaptation but also to changing the expectation of motor commands, i.e. updating the forward model. On the other hand, cerebellar patients reported the hand position without the shift, indicating that, unlike in healthy subjects, sensory-motor training did not alter their expectation of motor commands. This result was fully reproduced in a similarly designed study on healthy subjects, whose cerebellar activity was perturbed using transcranial direct current stimulation (Yavari et al., 2016).

Taken together, the aforementioned loss-of-function studies support the hypothesis that the cerebellum functions as a forward model that predicts consequences of motor commands and improves state estimation.

1.3 Larval zebrafish as a model organism to study adaptive behavior

Larval zebrafish (*Danio rerio*) possess a unique combination of advantageous features that have recently made them a powerful model in system neuroscience. On one hand, their small size, translucency and ability to survive immobilization for a long time opens up opportunity for minimally invasive optogenetic manipulation and whole-brain functional imaging using two-photon, light-sheet or light-field microscopy in awake and behaving animals. On the other hand, despite their small size and young age, larval zebrafish exhibit a rich behavior repertoire ranging from innate behaviors such as optomotor response (Neuhauss et al., 1999), optokinetic response (Easter and Nicola, 1997), visual startle response (Burgess and Granato, 2007; Easter and Nicola, 1997), and rheotaxis (Oteiza et al., 2017), to more complex behaviors such as prey capture (Borla et al., 2002; McElligott and O’malley, 2005), adaptation of locomotion (Portugues and Engert, 2011) and associative learning (Aizenberg and Schuman, 2011; Hinz et al., 2013; Li, 2012). Moreover, the zebrafish provides easy genetic access enabling usage of multiple molecular tools in a tissue-specific manner.

1.3.1 Cerebellum in larval zebrafish

As a typical representative of vertebrates, larval zebrafish have a cerebellum, and the main cerebellar cell types as well their morphological organization and synaptic connections are similar to what was described above (Introduction section 1.2.1). The only major difference is that in teleost fish, the main efferent output neurons, termed eurydendroid cells (ECs), are not piled in DCN but rather segregated in the PC layer while exhibiting many features similar to DCN neurons (Ikenaga et al., 2006). As mentioned above, powerful molecular tools available in the larval zebrafish model enable genetic access to specific populations of neurons, including cells of the olivo-cerebellar system (Figure 1.4).

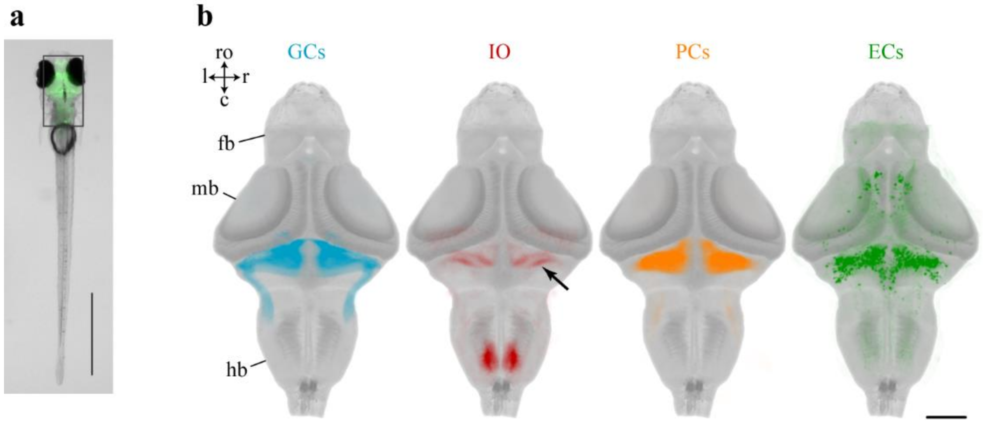

Figure 1.4. Olivo-cerebellar cells in the larval zebrafish brain

a. Microphotograph of a larval zebrafish expressing GCaMP6s under a pan-neuronal promotor. Scale bar denotes 1 mm. Gray rectangle outlines the area shown in **b**. **b**. Transgenic lines that specifically label different olivo-cerebellar cell types, overlaid with a larval zebrafish reference brain; ro – rostral direction, l – left, r – right, c – caudal; fb – forebrain, mb – midbrain, hb – hindbrain. Colors are the same as in Figure 1.3. Black arrow indicates the CFs. Scale bar denotes 100 µm. For transgenic lines used in this panel, see Materials and methods section 2.1.2.

1.3.2 Adaptive behavior in larval zebrafish

If a larval zebrafish is presented with a moving stimulus, it will turn and swim in the direction of perceived motion in order to stabilize its position with respect to the visual environment: a behavior termed optomotor response (OMR) (Neuhauss et al., 1999). At the larval stage, zebrafish move their tail not continuously but rather in discrete episodes called swimming bouts. A typical swimming bout can comprise several full tail oscillations and last ~ 350 ms. Bouts are elicited at a frequency of ~ 1 Hz and are separated by quiescent periods called interbouts (Budick and O'Malley, 2000).

Portugues and Engert (2011) developed a virtual-reality assay, in which a head-restrained zebrafish larva performs OMR to a forward-moving black-and-white grating, and when it swims, the grating speed changes in a closed-loop manner. Therefore, in this assay, animals have some control over their visual environment, and by changing their behavior, they are able to change the visual feedback that they receive. Importantly, feedback does not only depend on behavior of the animals, but it is also under experimental control. Experimenters can change the rules that determine how a given behavioral output is converted into visual feedback. For example, one can decrease the gain of the closed feedback loop, thus making the animals "slower". This allowed the authors to demonstrate that larval zebrafish are able to adapt their swimming behavior depending on visual feedback that they receive. Namely, increases and decreases in the gain of the closed feedback loop resulted in generalized decrease or increase of motor output, respectively. For example, when the gain was low (i.e. when the animals were "slow"), zebrafish larvae swam in longer and more frequent bouts. This adaptation was acute, in a sense that it occurred rapidly within the time course of individual swimming bouts, as opposed to long-term motor learning, when several trials are required to modify the behavior. The authors suggested that swimming larval zebrafish have an internal representation of visual feedback that it expects to see after a given motor command, and if the real feedback does not meet this expectation, the animals adapt their behavior to minimize this discrepancy. This is equivalent to proposing that larval zebrafish use forward models for acute adaptation of the OMR.

In a different study (Ahrens et al., 2012), whole brain calcium activity was recorded using two-photon functional imaging in animals performing adaptive OMR in a similar closed-loop assay. The olivo-cerebellar system was demonstrated to be involved in acute OMR adaption. Since the olivo-cerebellar system is a likely neuronal substrate for forward models (see Introduction section 1.2.2), this study supports the idea that internal models are used by larval zebrafish during acute OMR adaptation.

1.4 Thesis objectives

The major goal of this study was to unravel the mechanisms underlying acute and long-term OMR adaptation in larval zebrafish, with specific focus on the role of the cerebellum in these processes. In accordance with this general goal, the following specific aims were formulated:

1. Characterize acute OMR adaptation by exposing zebrafish larvae to different perturbations in visual reafference.
2. Test the requirement of the cerebellum in acute OMR adaptation by performing targeted ablation of PCs and testing PC-ablated animals in the acute adaptation experiment.
3. Since the results of acute adaptation experiments suggested that this process is likely to be implemented by a feedback controller, the next aim was to design such controller that would reproduce observed acute behavioral changes. The designed controller was based on the process of integrating sensory evidence in time, so the next related aim was to test whether the larval zebrafish brain indeed performs this integration. To this end, whole-brain functional imaging was employed.
4. Develop long-term OMR adaptation assay and characterize behavior of larval zebrafish in this assay.
5. Test the requirement of the cerebellum in long-term OMR adaptation.

2. Materials and methods

2.1 Model organism and subject details

2.1.1 Zebrafish husbandry

All experiments were conducted on larval zebrafish (*Danio rerio*) at 6 - 7 days post-fertilization (dpf) of yet undetermined sex. All animal procedures were performed in accordance with approved protocols set by the Max Planck Society and the local government (Regierung von Oberbayern; TVA 55-2-1-54-2532-82-2016).

Both adult animals and larvae were maintained at 28 °C on a 14/10 hour light/dark cycle, unless specified otherwise (Materials and methods section 2.1.3). Adult zebrafish were kept in a zebrafish facility system of Max Planck Institute of Neurobiology with constantly recirculating water with a daily 10% fresh water exchange. The zebrafish facility media was deionized water adjusted with synthetic salt mixture (Instant Ocean) to 600 µS conductivity, and the pH value adjusted to 7.2 using $NaHCO_3$ buffer solution. The water was filtered over bio-, fine- and carbon filters and UV-treated during recirculation. Adult zebrafish were fed twice a day with a mixture of artemia and flake feed.

To obtain larvae for experiments, 1 male and 1 female (in some cases, 3 male and 3 female) adult zebrafish were placed in a mating box in the afternoon and kept there overnight. The embryos were collected in the following morning and placed in an incubator that was set to maintain the above light and temperature conditions (Binder, Germany). Embryos and larvae were kept in 94 mm Petri dishes at a density of 20 animals per dish in Danieau's buffer solution (58 mM NaCl, 0.7 mM KCl, 0.4 mM $MgSO_4$, 0.6 mM $Ca(NO3)_2$, 5 mM HEPES buffer) until 1 dpf and in zebrafish facility system water from 1 dpf onwards. The water in the dish was changed daily.

2.1.2 Zebrafish strains

For purely behavioral experiments, I used wild-type Tüpfel long-fin (TL) zebrafish strain. Additionally, to test the behavior of animals with impaired cerebellar function, I used transgenic *PC*:epNtr-tagRFP animals (see Materials and methods section 2.1.3 for details about this line and the ablation method).

For functional imaging experiments, I used transgenic zebrafish that express GCaMP6s under a pan-neuronal promotor *elavl3* (*elavl3*:GCaMP6s) (Kim et al., 2017). To enable better optical access to the brain, I used animals with *nacre* mutation. This mutation introduces a deficiency in *mitfa* gene that is involved in development of melanophores (Lister et al., 1999). As a result, *nacre* mutants (*mitfa*$^{-/-}$) lack optically impermeable pigmented spots on the skin.

To demonstrate different cerebellar cell populations in the larval zebrafish brain (Figure 1.4), I used the following gene/enhancer trap transgenic lines (published in Takeuchi et al., 2015) that express a modified version of Gal4-VP16 (GFF) specifically in respective population of neurons:

- GCs - gSA2AzGFF152B; UAS:mCherry and hspGFFDMC90A; UAS:mCherry
- IO and CFs - hspGFFDMC28C; UAS:GFP
- ECs - hspzGFFgDMC156A; UAS:mCherry
- To show PCs, I used a line that expresses gap43-mCherry directly under PC-specific promotor *aldoca* (*aldoca:*gap43-mCherry).

All animals also carried homozygous *nacre* mutation. Several larvae from each of these lines were imaged under a confocal microscope (Carl Zeiss, Germany), co-registered and averaged together (see Materials and methods section 2.5.3 for details about anatomical registration).

To present functional imaging results and expression patterns of the transgenic lines listed above within the context of larval zebrafish gross neuroanatomy, I registered these data to a common reference brain. The reference brain stack was previously obtained in the lab by co-registration and averaging 23 confocal stacks of larval zebrafish brains that express GCaMP6f under *elavl3* promotor (*elavl3*:GCaMP6f) (Wolf et al., 2017), homozygous for *nacre* mutation.

Finally, to evaluate the efficiency of PC ablation, I outcrossed the *PC*:epNtr-tagRFP line with zebrafish that expressed GCaMP6s specifically in PCs' nuclei (Fyn-tagRFP:*PC*:NLS-GCaMP6s) (Knogler et al., 2019). This allowed observing the effects of the ablation protocol not only on the membrane morphology, but also on the morphology of cell nuclei (see Materials and methods section 2.1.3 for details).

All transgenic lines used in this thesis are listed in Table 1.

Name of the line	Expression pattern	Expressed molecule	Purpose of use	Reference
TL	-	-	Behavioral experiments: wild-type control group	-
PC:epNtr-tagRFP	PCs	epNtr and membrane-tagged RFP	Behavioral experiments: treatment control and PC ablation groups	Markov et al. (submitted)
Fyn-tagRFP:*PC*:NLS-GCaMP6s		Membrane-tagged RFP and nucleus-localized GCaMP6s	Evaluation of efficiency of PC ablation protocol	Knogler et al., 2019
elavl3:GCaMP6s	Pan-neuronal	GCaMP6s	Functional imaging experiments	Kim et al., 2017
elavl3:GCaMP6f		GCaMP6f	Reference brain	Wolf et al., 2017
gSA2AzGFF152B; UAS:mCherry	GCs	mCherry	Demonstration of cerebellar cell populations in larval zebrafish brain	Takeuchi et al., 2015
hspGFFDMC90A; UAS:mCherry				
hspzGFFgDMC156A; UAS:mCherry	ECs			
*aldoca:*gap43-mCherry	PCs			
hspGFFDMC28C; UAS:GFP	IO cells, CFs	GFP		

Table 1. Zebrafish strains used in this thesis

2.1.3 Targeted pharmaco-genetic ablation of PCs

(contribution of Andreas Kist)

The core of this thesis is testing adaptive behaviors in animals with impaired cerebellar function. To this end, I employed Ntr/MTZ pharmaco-genetic approach that has been successfully used in zebrafish (Curado et al., 2007; Pisharath et al., 2007; Tabor et al., 2014). This method is based on expressing an enzyme nitroreductase (Ntr) in a cell population-to-be-ablated and treating the animals with prodrug Metronidazole (MTZ). Ntr converts MTZ into a cytotoxic DNA cross-linking agent leading to death of cells that express Ntr. My fellow PhD student Andreas Kist generated a transgenic line that expressed enhanced Ntr (epNtr) (Tabor et al., 2014) under the PC-specific *carbonic anhydrase 8* (*ca8*) enhancer element (Matsui et al., 2014). Andreas cloned epNtr fused to tagRFP (similar to Tabor et al., 2014) downstream to the *ca8* and a basal promoter. He then injected this construct, abbreviated as *PC*:epNtr-tagRFP, into single-cell stage wild-type TL embryos heterozygous for *nacre* mutation, at a final concentration of 20 ng/µl together with 25 ng/µl *tol2* mRNA. Larvae showing strong expression of tagRFP in PCs were raised to adulthood as founders and outcrossed to gain a stable line.

To identify ablation-induced changes in adaptive behavior, I used the progeny of a single founder. The embryos obtained from *PC*:epNtr-tagRFP$^{+/-}$ strain outcrossed to a TL fish were screened for red fluorescence in the cerebellum at 5 dpf, and 10 positive (*PC*:epNtr-tagRFP$^{+/-}$) and 10 negative (*PC*:epNtr-tagRFP$^{-/-}$) larvae were kept in the same Petri dish to ensure subsequent independent sampling. At 18:00, most of the water in the dish was replaced with 10 mM MTZ solution in zebrafish facility water, and larvae were incubated in this solution overnight in darkness for 15 hours. The next morning at 9:00, animals were allowed to recover in fresh fish water. The next day, adaptive behavior of 7 dpf MTZ-treated larvae was tested under respective behavioral protocol (Materials and methods section 2.3.1). After the experiment, the larvae were screened for red fluorescence once again to reassess their genotype after mixing positive and negative larvae in one Petri dish. *PC*:epNtr-tagRFP$^{-/-}$ and *PC*:epNtr-tagRFP$^{+/-}$ siblings constituted treatment control and PC ablation groups, respectively.

The quality of PC ablation was evaluated by imaging progeny of *PC*:epNtr-tagRFP fish outcrossed to Fyn-tagRFP:*PC*:NLS-GCaMP6s fish under a confocal microscope (Carl Zeiss, Germany).

2.2 Closed-loop experimental assay in head-restrained preparations

Both behavioral and functional imaging experiments were conducted using closed-loop virtual reality assay in head-restrained preparations of 6-7 dpf zebrafish larvae, similar to Portugues and Engert (2011) (see also Introduction section 1.3.2). For behavioral experiments, each larva was embedded in 1.5 % low melting point agarose (Invitrogen, Thermo Fisher Scientific, USA) in a 35 mm Petri dish. For functional imaging experiments, larvae were embedded in 2.5 % agarose in custom-built plastic chambers, with glass coverslips sealed with grease on the front and right sides of the chamber, at the entry points of the frontal and lateral laser excitation beams, and the agarose around the head was removed with a scalpel to avoid scattering of the beams (see Materials and methods section 2.5.1 for details about functional imaging setup). After allowing the agarose to set, the dish/chamber was filled with zebrafish facility water and the agarose around the tail was removed to enable unrestrained tail movements that were subsequently used as a behavioral readout.

A dish/chamber with an embedded larva was then placed onto the screen of the custom-built behavioral or functional imaging rig (Figure 2.1a). In the behavioral rig, the screen with the dish was illuminated from below by an infrared (IR) light-emitting diode (LED) (not shown in Figure 2.1a). A square black-and-white grating with a spatial period of 10 mm was projected onto the screen by a commercial Digital Light Processing projector (ASUS, Taiwan). Larvae were imaged through a macro objective (Navitar, USA) and an IR-pass filter with an IR-sensitive camera (Pike, Allied Vision Technology, Germany, or XIMEA, Germany) at 200 frames per second. The functional imaging rig was built in a similar way, with the two differences:

1. IR LED illuminating the chamber was directed from above and the image was reflected on a hot mirror to reach a camera (XIMEA, Germany).
2. the projector used to provide visual stimulation (Optoma, USA) was mounted with a red-pass filter to avoid bleed-through in the light collection optics.

Stimulus presentation and tail tracking were controlled by the open-source, integrated system for stimulation, tracking and closed-loop behavioral experiments (Stytra) (Štih et al., 2019). One trial consisted of a 15-second presentation of the grating moving in a caudal to rostral direction at 10 mm/s, preceded and followed by 7.5-second periods of the static grating (Figure 2.1c, top magenta trace). Before starting an experiment, two anchor points enclosing the tail were manually selected. The tail between the anchor points was divided into 8 equal segments, and the angle of each segment was automatically detected by Stytra in real time. The cumulative sum of the tail segment angles constituted the final tail trace (Figure 2.1c, top green trace). Sliding standard deviation of the tail trace with a time window of 50 ms was computed in real time, and the resulting parameter will be referred to as vigor. Vigor is close to zero when larvae do not move their tail and increase when they do, and can be therefore used to estimate the forward velocity that larvae would have reached if they were not head-restrained (Figure 2.1c, bottom green trace). To this end, the vigor trace was multiplied by a factor that was optimized so that that the median estimated speed during a typical bout was 20 mm/s, that corresponds to a freely swimming situation. The estimated velocity was subtracted from the initial grating speed to provide visual reafference to the behaving larvae (Figure 2.1c, bottom magenta trace). As a result, animals could experience the effects of their own swimming. The initial and actual grating speeds, tail trace, vigor and reafference condition (see below) at each time point constituted the raw data saved after an experiment (Figure 2.1c).

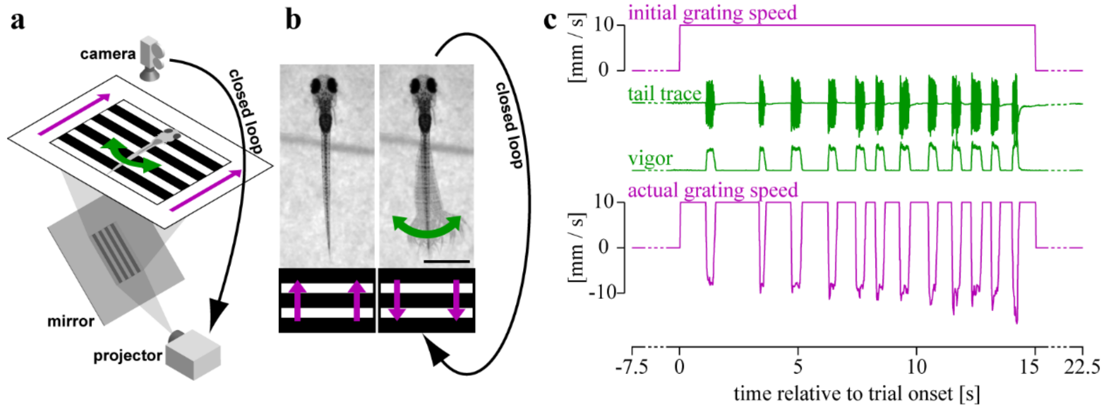
a
b
c
camera
closed loop
mirror
projector
closed loop
[mm / s]
10
0
initial grating speed
tail trace
vigor
actual grating speed
[mm / s]
10
0
-10
-7.5
0
5
10
15
22.5
time relative to trial onset [s]

Figure 2.1. Closed-loop experimental assay and an example trial

a. Experimental setup. A head-restrained larva is presented with a moving grating by a projector. Direction of the grating motion is indicated by the magenta arrows. Resulting tail movements (indicated by the green arrow) are imaged by a high-speed camera and fed back to the stimulus, thus closing the loop. Zebrafish, stimulus and the setup are shown not to scale for illustration purposes. **b**. Closed-loop experimental approach. When a larva moves its tail, the grating speed changes, providing visual reafference to the behaving larva. Scale bar denotes 1 mm. The gratings below the fish are shown not to scale for illustration purposes. Images of a zebrafish larva were obtained through the behavioral camera shown in **a**. **c**. Raw data traces from one example trial. *Figure adapted from Markov et al. (submitted).*

Importantly, in such closed-loop assay, experimenters have control over the rules that determine how estimated fish velocity translates to changes in visual reafference. In Figure 2.1c, the rules were set so that visual reafference mimics what a freely swimming larva usually experiences. Changing these rules enables to study how visual reafference affects behavior. During experiments, I used perturbations in visual reafference that fall into three distinct conditions designed to test different features (Figure 2.2):

1. The first reafference condition, that has been previously used in the literature (Ahrens et al., 2012; Portugues and Engert, 2011), will be referred to as *gain change*. It corresponds to changing the gain of the experimental closed loop, such that larvae receive more or less sensory feedback when they swim (Figure 2.2a). The gain values used in this study included 0, 0.33, 0.66, 1, 1.33, 1.66, and 2. Note that a gain of 0 corresponds to *open loop* and a gain of 1 to freely swimming conditions that will be referred to as *normal reafference*.
2. The second condition was called *lag*, and this corresponds to introducing an artificial temporal delay between the behavior of the larva and the reafference it experiences (Figure 2.2b). In the *shunted lag* version of this condition, the reafference was automatically set to zero when the larvae stop swimming. The lag values used in this study included 0, 75, 150, 225, 300 ms, and infinite lag (i.e. reafference never arrives after the bout onset, that is equivalent to the open loop condition). The *lag* conditions test how the temporal relationship between the behavior and resulting reafference affects the former.
3. The final reafference condition was originally developed by my fellow PhD student Andreas Kist and was termed *gain drop*. It corresponds to dividing the first 300 ms of a bout into four 75 ms segments and setting the gain during one or more of these segments to 0 (Figure 2.2c). For example, the gain drop profile 1100 means that the gain during segments 3 and 4 (i.e. from 150 ms to 300 ms after the bout onset) was

set to 0, and during the rest of the bout it was set to 1. Gain drop profiles used in this study included 1111, 0111, 0011, 0001, 0000, 1110, 1100, and 1000. The *gain drop* condition tests whether reafference changes lead to same behavioral adaptations regardless of when they occur within the bout.

No combinations of reafference conditions were used, e.g. if the gain was set to 0.33, the lag was automatically set to zero, or if the lag was set to 225 ms, the gain was set to 1, and in both cases the gain drop profile was set to 1111.

Note that reafference conditions listed above and presented in Figure 2.2 are redundant. For example, the gain drop profile 0011 is exactly the same as 150 ms shunted lag, or gain 0 is exactly the same is infinite lag. Reafference conditions are presented here in a redundant way to highlight that infinite lag makes a logical sense at the end of the list of lag conditions, and gain 0 makes a logical sense in the beginning of the gain list. The exact list of reafference conditions (18 conditions in total) is the following:

1. normal reafference (gain 1, 0 ms lag, and gain drop 1111)
2. open loop (gain 0 or infinite lag)
3. gains: 0.33, 0.66, 1.33, 1.66, 2 (0 ms lag, and gain drop 1111)
4. lags and shunted lags: 75 ms, 150 ms, 225 ms, 300 ms (gain 1)
5. gain drops: 1110, 1100, 1000 (0 ms lag)

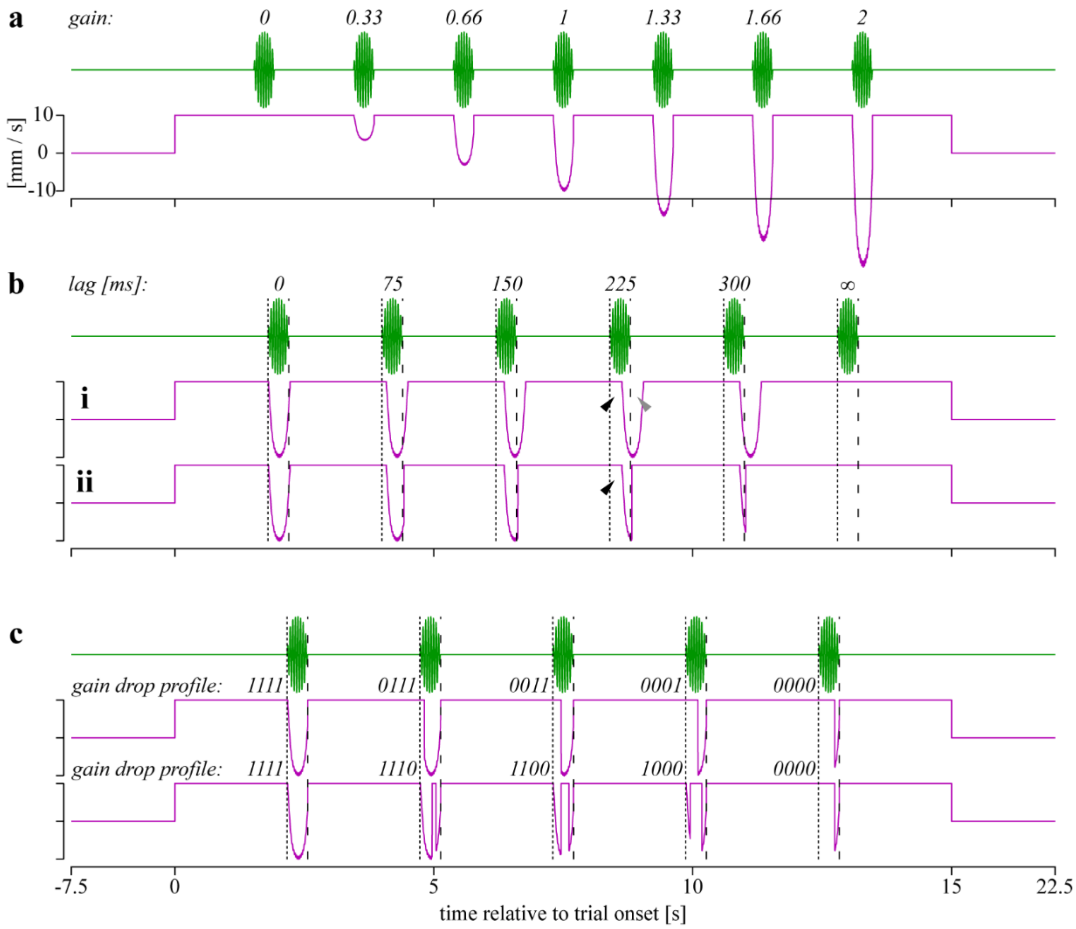

Figure 2.2. Reafference conditions used in this thesis

Example trials illustrating all reafference conditions used in this study. These trials were artificially composed for illustration purposes. Green and magenta denote tail traces grating speed, respectively. Dotted dashed lines denote bout onsets and offsets, respectively. **a**. Gains of the closed loop. **b**. Lags of the reafference; **i** – normal lag, **ii** – shunted lag. Note the difference between the normal and the shunted lag settings: in both cases there is insufficient reafference in the beginning of the bout (indicated by black arrowheads), whereas only in the non-shunted setting there is excessive reafference after the bout offset (indicated by gray arrowhead). **c**. Gain drop profiles.

2.3 Behavioral experiments

2.3.1 Experimental protocols

The first aim of this study was to investigate how larval zebrafish acutely adapt their behavior to different reafference condition. Acute adaptation experimental protocol consisted of 240 trials that were divided into 4 phases (see definition of a trial in Materials and methods section 2.2):

1. Calibration phase (trials 1:10). During this phase, the vigor multiplication factor (Material and methods section 2.2) was automatically calibrated so that the median estimated speed during an average swimming bout was 20 mm/s. Reafference condition during this phase was set to normal. The calibration was implemented to minimize across-subject variability in the virtual speed that could potentially result from uncontrolled differences in manipulations during embedding larvae in agarose and in placement of the Petri dishes into the rigs. In addition, during this phase, larvae could get used to the experimental environment and bring their swimming behavior to a stable level.
2. Pre-adaptation phase (trials 11:20). During this phase, reafference condition was set to normal.
3. Adaptation phase (trials 21:230). During this phase, reafference condition for each bout was randomly selected from the list of 18 possible reafference conditions (Materials and methods section 2.2 and Figure 2.2).
4. Post-adaptation phase (trials 231:240). During this phase, reafference condition was the same as during the pre-adaptation phase.

Another aim was to investigate long-term motor adaptation, when the same reafference condition is presented consistently over a long period of time. Long-term adaptation experimental protocol had a general structure similar to the acute adaptation experiments with the only difference that all reafference conditions during the adaptation phase were either normal (normal-reafference control animals), or 225 ms lag (lag-trained animals).

Python code of behavioral experiment protocols is available at our GitHub repository: https://github.com/portugueslab/Markov-et-al-2019,

2.3.2 Behavioral data analysis

Analysis of the behavioral data was performed in MATLAB (MathWorks, USA).

Tail trace was z-scored and interpolated together with the grating speed trace to a new time array with sampling period of 5 ms. For each swimming bout automatically detected by Stytra during the experiment, individual tail flicks were detected. One tail flick was defined as a section of the tail trace between two adjacent local extrema with the magnitude greater than 0.14 and the duration not greater than 100 ms (these thresholds were manually adjusted to ensure accurate bout detection). The automatically detected onsets and offsets of the bouts were then corrected to match the beginning of the first flick and the end of the last flick, respectively.

For further analysis, I only considered bouts that occurred while the grating was moving (i.e. spontaneous bouts were excluded). For each bout, I computed its duration and duration of the subsequent interbout. If a bout was the last in a trial, its interbout duration was replaced with a NaN value. All bouts that were shorter than 100 ms, or had a subsequent or preceding interbout duration shorter than 100 ms were also excluded from the analysis.

If the number of remaining bouts performed by a given larva was less than 540, this animal was excluded from the analysis. Additionally, if there was at least one block of 10 trials with zero bouts, the animal was also excluded. The final numbers of animals included in the analysis are presented in Table 2.

Experiment	Experimental group	Genotype	Treatment	*N*
Acute adaptation	Wild-type control	TL	-	100
	Treatment control	*PC*:epNtr-tagRFP$^{-/-}$	MTZ	28
	PC ablation	*PC*:epNtr-tagRFP$^{+/-}$	MTZ	39
Long-term adaptation (normal reafference)	Wild-type control	TL	-	103
	Treatment control	*PC*:epNtr-tagRFP$^{-/-}$	MTZ	85
	PC ablation	*PC*:epNtr-tagRFP$^{+/-}$	MTZ	83
Long-term adaptation (225 ms lag)	Wild-type control	TL	-	100
	Treatment control	*PC*:epNtr-tagRFP$^{-/-}$	MTZ	85
	PC ablation	*PC*:epNtr-tagRFP$^{+/-}$	MTZ	90

Table 2. Numbers of animals tested in the behavioral experiments

To analyze the temporal dynamics of the tail beat amplitude within individual bouts, I selected, for each bout, a 1.1-second long section of the tail trace, starting from 100 ms before the bout onset. The values of the tail trace within the section after the bout offset were replaced with NaN values to exclude the contamination by subsequent bouts that could occur during the section. The tail trace within the sections was then squared and termed the *bout power*. Based on the observed results (see Results section 3.1.4), the sections were divided into ballistic and reactive periods (from 0 to 220 ms after the bout onset and from 220 ms onward, respectively) and the areas below the bout power curves within these two periods were computed.

All behavioral results in this study are presented as mean values ± standard error of mean (SEM) across animals, unless otherwise specified. To present the results of acute adaptation experiments, I computed mean bout and interbout duration, as well as the bout power profile and areas below the bout power curve during ballistic and reactive periods, for each reafference condition for each subject. To present the results of long-term adaptation experiments, I measured the aforementioned parameters only for the first bout in each trial assuming that the first bout should not depend on putative short-term sensory-motor memory accumulated during the trial and should therefore reflect long-term changes in circuitry involved in OMR better than the subsequent bouts. To quantify the long-term adaptation effects, I divided all trials of the protocol into blocks of 10 and computed the mean value of respective parameter for blocks that correspond to pre-adaptation phase, post-adaptation phase, and the last 10 trials of the adaptation phase.

Since the samples were not expected to come from populations with normal distributions, the nonparametric Mann-Whitney U test was used to estimate statistical significance of the observed differences, with significance level of 5 %.

2.4 Modelling a feedback controller of acute adaptation

2.4.1 Designing the model

To test whether acute OMR adaptation can be explained by a simple feedback control mechanism that does not involve computation of predicted sensory feedback (i.e. forward models), I developed a model that does not perform these computations (Figure 3.8a). The model was developed and tested in MATLAB (MathWorks, USA). The input of the model was the grating speed and the previous state of the model nodes, and the output was binary motor variable: swim or no swim. For simplicity, I did not model individual tail flicks as the model’s output and approximated the swimming behavior of the zebrafish larvae by a binary motor output, that equals 1 when the fish is swimming and 0 otherwise. This was possible due to discrete nature of zebrafish swimming behavior at larval stage. Since in this study I focused only on duration of bouts and interbouts, while ignoring other motor parameters such as tail beat amplitude and frequency, this simplification did not limit the ability to compare the model behavior with behavior of the real larvae. To design the model, I used the results of the acute adaptation experiment as a starting point (Results section 3.1). Thus, since larval zebrafish react to changes in visual stimulus with a fixed delay of 220 ms, the input of the model at a given time point was the grating speed 220 ms before that point. Since acute adaptation to different gains suggested that larval zebrafish are able to detect the direction of the grating motion and the adaptation depended on this direction, the first step of the model was splitting the input signal into positive and negative components by rectification. Rectification was performed by two respective model nodes: forward and reverse motion sensors (FMS and RMS, respectively). I then proceeded from the fact that when a larval zebrafish is presented with a forward moving grating, it performs a swimming bout only after a certain latency period, suggesting that it integrates sensory evidence in time until the level of integration reaches a motor command threshold. I therefore introduced a leaky sensory integrator (SI) that integrates inputs from the motion sensors. Since the results of the acute adaptation experiment suggested that forward motion of the stimulus is associated with increased swimming, and reverse motion with decreased swimming, the input from the FMS to the SI was excitatory, and from the RMS – inhibitory. The SI excited the motor output generator (MOG), and when activity of the latter exceeded a threshold, the motor command was generated and the output of the model was set to 1. To ensure that the swimming bouts of the model do not last forever, I added a leaky motor integrator (MI) that integrates the motor output and inhibits the MOG. Thus, by introducing the MI, I reproduced a self-evident fact that the longer a bout has been, the sooner it will stop. Finally, to ensure that the bouts are never infinitely short, I added a feed-forward loop to the motor output, so that it can excite itself. Therefore, if after a bout onset, activity of the SI and the MOG dropped below the motor output command threshold (due to a very high gain of the closed loop, for example), the bout would nonetheless continue for some time. Input and output of the model, as well as activity of its nodes in one example trial are presented in Figure 3.8. The mathematical equations defining behavior of the model are listed below, and the MATLAB code of the model is available in Appendix 5.3.

- $FMS(t) = [In(t - 220\,ms)]_+$
- $RMS(t) = -[In(t - 220\,ms)]_-$
- $\tau_s * \frac{dSI(t)}{dt} = \omega_f * FMS(t) - \omega_r * RMS(t) - SI(t-1)$
- $SI(t) = min([SI(t)]_+, 1)$
- $MOG(t) = SI(t) - \omega_i * MI(t-1)$
- $Out(t) = 1\ if\ MOG(t) + \omega_s * Out(t-1) > thr\ and\ 0\ otherwise$
- $\tau_m * \frac{dMI(t)}{dt} = \omega_m * Out(t) - MI(t-1)$
- $MI(t) = min(MI(t), 1)$

$t -\ current\ time\ point, t-1 - previous\ time\ point$

$In - input\ of\ the\ model\ (grating\ speed, where\ positive\ values\ correspond\ to$
$motion\ in\ a\ caudal\ to\ rostral\ direction)$

$Out\ -\ output\ of\ the\ model\ (binary\ swimming\ variable)$

$[x]_+ = max(x, 0) - positive\ rectification\ of\ x$

$[x]_- = min(x, 0) - negative\ rectification\ of\ x$

$min(x, 1) - saturation\ of\ x\ at\ 1$

$\omega_f\ -\ forward\ input\ weight\ of\ the\ sensory\ integrator$

$\omega_r\ -\ reverse\ input\ weight\ of\ the\ sensory\ integrator$

$\tau_s\ -\ time\ constant\ of\ the\ sensory\ integrator$

$\omega_i\ -\ output\ weight\ of\ the\ motor\ integrator$

$\omega_s\ -\ weight\ of\ feedforward\ self\ escitation\ of\ the\ output\ node$

$thr\ -\ threshold\ of\ the\ motor\ output\ command$

$\omega_m\ -\ input\ weight\ of\ the\ motor\ integrator$

$\tau_m\ -\ time\ constant\ of\ the\ motor\ integrator$

2.4.2 Fitting and testing the model

To evaluate the ability of the model to acutely adapt to changes in reafference, I tested its performance in a shorter version of the acute adaptation experimental protocol (Materials and methods section 2.3.1). The protocol was shortened to reduce computation time required for fitting the model parameters to the real data. One trial consisted of 300 ms of static grating followed by 9.7 second of the grating moving in a caudal to rostral direction at 10 mm/s. The reafference condition of the first bout was always normal, and the reafference condition of the second bout was chosen from a list of 18 reafference conditions used in the acute adaptation experiment (Materials and methods section 2.2). If the model initiated a third bout within the allowed 10 seconds of the trial, the trial was terminated, and the duration of the second bout and subsequent interbout duration constituted the final output of the model in that trial. If the model did not perform the third bout, the final output of the model in that trial was replaced with NaN values. One experiment consisted of 18 trials probing behavior of the model under each reafference condition.

The parameters of the model were fitted to each larva that participated in the acute adaptation experiment using a custom-written genetic algorithm. To obtain the training datasets, I generated 18 arrays of bout durations and 18 arrays of interbout durations for each larva, each array corresponding to one reafference condition. I then randomly selected 50 % from each array, and computed their mean values. I will refer to the remaining 50 % as test datasets.

The fitting algorithm minimized the mean absolute error (absolute difference between the output array of the model and a training dataset, normalized by the training dataset). The fitting resulted in sets of the model parameters, each optimized to fit one larva. To present the results, I computed the mean values and SEM of the final output arrays of models across all sets of parameters, and of the test datasets across all larvae.

2.5 Functional imaging experiments

(contribution of Luigi Petrucco)

2.5.1 Light sheet microscope

To test the main assumption of the proposed feedback control model of acute adaptation: the existence of the sensory integration in the larval zebrafish brain, I employed whole-brain calcium imaging using a custom-built light-sheet microscope (Figure 2.3a). In the microscope, a beam coming from a 473 nm laser source (modulated laser diodes, Cobolt, Sweden) was split with a dichroic mirror and conveyed to two orthogonal scanning arms. Each scanning arm consisted of a pair of galvanometric mirrors (Sigmann Electronik, Germany) that allowed vertical and horizontal scanning of the beam, a line diffuser (Edmund Optics, USA), a scan lens (Thorlabs, USA), a paper screen to protect the fish eyes, a tube lens (Thorlabs, USA), and a low numerical aperture objective (Olympus, Japan). The emitted light was collected through a water immersion objective (Olympus, Japan) mounted on a piezo (Piezosystem Jena, Germany), bandpass filtered (AHF Analysentechnik, Germany), and focused on the camera with a tube lens (Thorlabs, USA). Images were recorded using an Orca Flash v4.0 camera (Hamamatsu Photonics K.K., Japan) with Camera Link.

The piezo, galvanometric mirrors, and camera triggering were controlled by a custom-written Python program. The light sheet was created by horizontal scanning of the laser beams at 800 Hz. The light sheet and the collection objective were constantly oscillating along the vertical axis with a saw tooth profile of frequency 1.5 Hz and amplitude of 250 µm. At each oscillation, 35 frames were acquired at equally spaced intervals; with an exposure time of 5 ms. The resulting raw volumetric videos had a voxel size of 7 x 0.6 x 0.6 µm, and a time sampling frequency of 1.5 Hz.

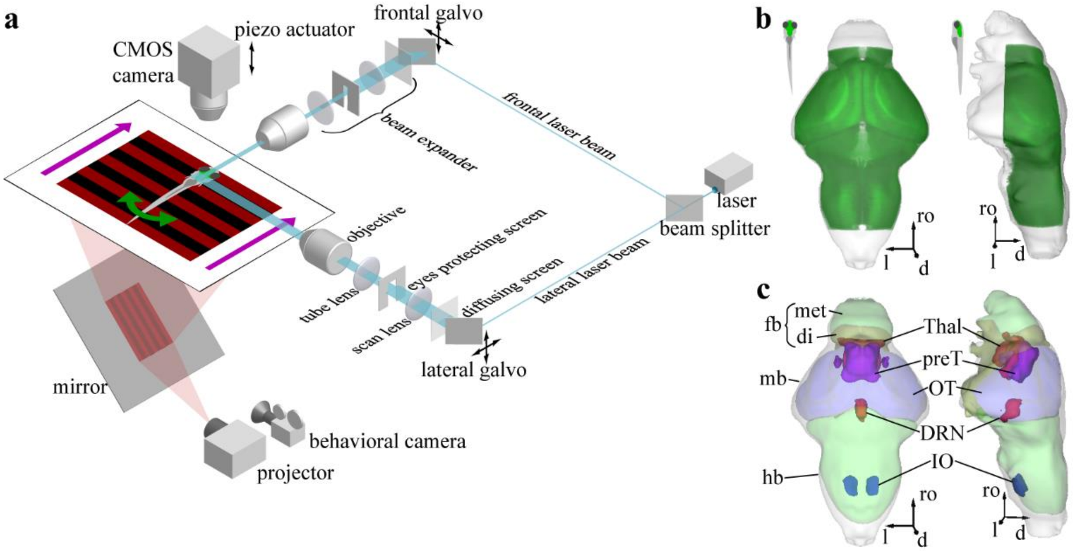
a
piezo actuator
CMOS camera
frontal galvo
beam expander
frontal laser beam
laser
beam splitter
objective
tube lens
eyes protecting screen
scan lens
diffusing screen
lateral laser beam
lateral galvo
mirror
behavioral camera
projector
b
ro
l
d
c
fb
met
di
mb
hb
Thal
preT
OT
DRN
IO

Figure 2.3. Light sheet setup and imaged brain area

a. Light-sheet microscope combined with a behavioral rig used in the functional imaging experiments (see details in the text of this section). The closed loop experimental assay is the same as in Figure 2.1. **b**. Dorsal and lateral view of 3D-rendered intersecting brain area that was imaged in all animals (see Materials and methods section 2.5.3); ro – rostral direction, d – dorsal, l – left. Transparent surface depicts the outline of the 3D-rendered reference brain; the length of the scale arrows is 100 µm. **c**. Selected anatomical regions that exhibited experiment-related activity, registered from the Z-Brain atlas (Randlett et al., 2015) to the reference brain: met – metencephalon, di – diencephalon, fb – forebrain (prosencephalon), mb – midbrain (mesencephalon), hb – hindbrain (rhombencephalon), Thal – thalamus, preT – pretectum, OT – optic tectum, DRN – dorsal raphe nucleus, IO – inferior olive. Panels **a** and **b** *adapted from Markov et al. (submitted).*

2.5.2 Experimental protocol

Functional imaging experimental protocol was similar to acute adaptation protocol (Materials and methods section 2.3.1). It started with 2 minutes of no stimulation to record spontaneous activity, followed by a calibration phase (10 trials), a pre-adaptation phase (10 trials) and an adaptation phase (40 trials) (see definition of a trial in Materials and methods section 2.2). In 2 out of 4 animals, the calibration phase was omitted because behavior under the light-sheet setup was less consistent than under the purely behavioral rigs, and calibration often failed due to low number of bouts performed during the calibration phase. For these larvae, the vigor multiplication factor (Materials and methods section 2.2) was set manually to the value obtained during successful calibration in a different larva. During the adaptation phase, reafference condition for each bout was randomly set to either normal or open loop. In addition, two 350-ms pulses of reverse grating motion (rostral to caudal direction) at 10 mm/s were presented during each static grating period (5 and 10 s after the grating stopped moving). These pulses were added to disambiguate motor-related activity from responses to reverse grating motion that accompanies closed-loop bouts. Responses to these pulses were not analyzed in this thesis.

Python code of the imaging experiment protocol is available at our GitHub repository: (https://github.com/portugueslab/Markov-et-al-2019).

2.5.3 Functional imaging data analysis

Behavioral data acquired during the imaging experiments was analyzed in the same way as for pure behavioral experiments (see Materials and methods section 2.3.2). This section only describes the analysis of the functional imaging data.

The imaging data was preprocessed in Python, similar to Kist et al. (2017). The preprocessing steps included aligning and segmenting the data into regions of interest (ROIs, see below) and were performed by my fellow PhD student Luigi Petrucco. To align the data, he first computed an anatomical reference volume by averaging the first 1000 frames of each plane. For each volume in time, the translation with respect to the reference volume was computed by cross-correlation using the *register_translation* function from the *scikit-image* Python package. Before alignment, Luigi filtered the reference volume and volumes to be registered with a Sobel filter after a Gaussian blur (standard deviation 3.3) to emphasize image edges over absolute pixel intensity. Volumes for which the computed shift was larger than 15 pixels (generally due to large motion artefacts caused by vigorous tail movements of the embedded fish) were discarded and replaced with Nan values. For subsequent registration of the imaging data to the common reference brain, a new anatomy stack was computed for each animal by averaging the first 1000 frames of the aligned planes.

To segment the imaged volume into ROIs, Luigi computed a "correlation map", where each pixel value equals the correlation between the fluorescence trace of that pixel and the average trace of the 8 adjacent pixels on the same plane. Then, based on the correlation map, individual ROIs were segmented for each plane with an iterative procedure. Each ROI was grown starting from the pixel with the highest intensity in the correlation map among the ones still unassigned to ROIs, with a minimum correlation of 0.3 (seed). Adjacent pixels were then gradually added to the growing ROI if eligible for inclusion. To be included, adjacent pixels correlation with the average fluorescence of the ROI grown until that point had to be above a set threshold. The threshold for inclusion was 0.3 for the first iteration and then it increased linearly as a function of the pixel distance to the seed, up to a value of 0.35 at 3-µm distance. Additional criteria for minimal and maximal ROI area (9-28 μm^2) ensured that the ROIs matched approximately the size of neuron somata. After segmentation, the fluorescence trace of each ROI was extracted by summing fluorescence of all pixels that were assigned to that ROI during segmentation.

I performed all subsequent analysis steps in MATLAB (MathWorks, USA). To denoise the trace, I applied a low-pass Butterworth filter with a cutoff frequency of 0.56 Hz, that corresponds to the 1.8 s half-decay time of the calcium indicator GCaMP6s used in the experiments (Chen et al., 2013), as fluorescence oscillations at frequency higher than 0.56 Hz were unlikely to result from biological events. To correct for potential slow baseline drift, I computed the trace's baseline by applying another low-pass Butterworth filter with a cutoff frequency of 3.3 mHz, and subtracted the baseline from the trace. The trace was then z-scored for subsequent analysis.

The subsequent analysis strategy was aimed to identify SIs within the larval zebrafish brain and included two main steps.

The first step was aimed to identify ROIs that responded to the forward moving grating. Since this stimulus reliably triggers swimming behavior, it was important to disambiguate ROIs with sensory responses from ROIs with motor-related activity. To this end, I computed the average grating- or bout-triggered fluorescence for each trace. To do this, I selected five second-long sections of the trace, starting from one second before the respective trigger. To avoid contamination of triggered averages by activity triggered by other events, I only considered triggers that did not have any other triggers up to one second before, and if another trigger occurred within the section, all fluorescence values after this other trigger were replaced with NaN values. In addition, I subtracted the baseline (fluorescence before the trigger within the section) from each triggered activity trace. I then computed the average traces and SEM across corresponding sections for each trace. To identify ROIs with sensory- and motor-related activity, I computed the mean values of average fluorescence triggered by grating onsets within the time window from 0 to 4 s with respect to the grating onset, and of average activity triggered by bout onsets within the time window from 0 to 2 s with respect to the bout onsets. These values were referred to as sensory and motor scores, respectively. If the sensory score of an ROI was greater than 0.4, this ROI was termed sensory, and if the sensory score was less than 0.1 and the motor score was greater than 0.2, the ROI was termed motor.

The second step was aimed to identify sensory ROIs that integrate sensory information in time. To this end, I fitted a leaky integrator model to average grating-triggered fluorescence of sensory ROIs by iterating over a range of time constants from zero to five seconds, with 100 ms steps, and identifying the time constant resulting in the highest correlation between the model and the triggered average trace. During the fitting procedure, the leaky integrator trace was additionally convolved with a GCaMP6s kernel, modeled as an exponential function with half-decay time of 1.8 s (Chen et al., 2013). Sensory ROIs for which the time constant was zero were termed sensors, whereas ROIs with time constants greater than zero were termed integrators.

To compare the location of ROIs assigned to the aforementioned functional groups between animals and to present the ROIs within the context of gross larval zebrafish neuroanatomy, I registered the imaging data to a common reference brain using the free Computational Morphometry Toolkit (Rohlfing and Maurer, 2003). To this end, affine volume transformations were computed to align the anatomical stacks from each larva to the reference brain. Aligned anatomical stacks were visually inspected, and if the registration failed, the larva was excluded from the analysis. This resulted in final $N = 4$ larvae. Computed transformations were applied to each ROI to identify its location in the reference space. In addition, the aligned anatomical stacks were used to identify the intersecting area that was imaged in all four animals (Figure 2.3b). ROIs outside this area were excluded from the analysis. To present the results, I summed registered ROI maps across fish, generated a 3D surface of the reference brain and rendered the ROI maps using 3D Viewer plugin for FIJI (Schindelin et al., 2012). Finally, to identify the anatomical regions with experiment-related activity, I registered the regions annotated in the Z-Brain atlas (Randlett et al., 2015) to our reference brain. Location of the selected anatomical regions is presented in Figure 2.3c.

3. Results

3.1 Acute OMR adaptation to changes in visual reafference

The first aim of this study was to characterize acute adaptation of the OMR to changes in visual reafference. By acute, I refer to changes in a bout in response to a perturbation in reafference during that same bout. To this end, I used a closed-loop experimental assay shown in Figure 2.1 (Materials and methods sections 2.2 and 2.3.1). Briefly, in this setting, a head-restrained larva performs swimming bouts in response to a forward moving grating. This behavior is captured by a high-speed camera and fed back to the stimulus so that the larva can experience the effects of its own swimming (i.e. receive visual reafference). The way in which the animal's behavior translates to changes in the visual stimulus is under experimental control. Reafference conditions used in this experiment included different *gain changes, shunted* and *non-shunted lags* of the reafference, and different *gain drops* (Materials and methods section 2.2). The order of reafference conditions was randomized in a bout-by-bout basis. In this section, I present mean bout duration, as well as duration of the following interbout, as a function of reafference condition during that bout.

3.1.1 Acute adaptation to gain of the closed loop

Changing the gain of the closed loop enables us to manipulate the virtual velocity with which a head-restrained larva progresses forward during a swimming bout (Figure 2.2a). Analysis of the mean bout duration as a function of this gain confirmed a previous report (Portugues and Engert, 2011) that lowering the gain leads to longer bouts (Figure 3.1a). This was particularly noticeable for the very low gains 0 and 0.33. It is interesting to note that for gains below 0.5, the larva's swimming did not reverse the direction of the forward moving grating (compare bout # 2 with bout # 3 in Figure 2.2a). Lowering the gain is equivalent to making the fish slower than normal (with respect to its visual environment), whereas lowering the gain to less than 0.5 makes the fish too slow to be able to progress forward at all. These two scenarios might have different ethological meanings for the fish, and this can underlie the more noticeable increase in bout duration for particularly low gains. However, further experiments are required to elucidate whether this fact underlies the observed trend.

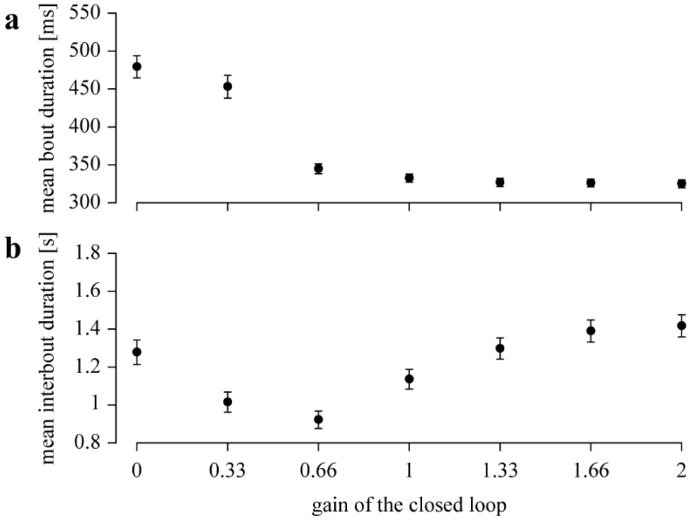

Figure 3.1. Acute OMR adaptation to gain of the closed loop

Mean bout duration (**a**) and interbout duration (**b**) as a function of gain of the closed loop. Black circles denote the mean values across subjects, error bars denote SEM, *N* = 100 larvae. *Figure adapted from Markov et al. (submitted).*

Regarding mean interbout duration, decreasing the gain from 2 to 0.66 results in shorter interbouts (Figure 3.1b). However, further decreases reverse this tendency to the extent that in the current experimental paradigm, interbouts at gain 0 were even longer than those at gain 1, in contrast with results obtained by Portugues and Engert (2011). This can be explained not only by the fact that gains 0.33 and 0 are too low for the larva to be able to progress forward, but also by the fact that bout duration at these gains was particularly high, and animals might have needed more interbout time to rest after these long bouts.

In summary, decreasing the virtual forward velocity of the animals (i.e. experimental gain of the closed loop) resulted in increased motor activity expressed as longer bouts and shorter interbouts. Furthermore, if the velocity becomes too low making it impossible for the animals to reverse the direction of the grating and progress forward, bouts become particularly long. This suggests that larval zebrafish are able to detect and acutely adapt their ongoing optomotor behavior to both amount of reafference that they receive and the direction of the stimulus motion during swimming.

3.1.2 Acute adaptation to lag of the reafference

In contrast to changing the gain of the closed loop, which enabled us to investigate how the *amount* of visual reafference affects behavior, lagging the reafference with respect to the bout onset keeps its amount unaltered while changing only the *temporal relationship* between the behavior and its visual feedback (Figure 2.2b). Lagging the reafference resulted in increased mean bout duration (Figure 3.2a). Interestingly, the increase in bout duration was close to linear as a function of the lag and, as expected, it did not show a significant difference between the lag and shunted lag cases, as these two conditions only differed in whether the speed of the forward moving grating returned to baseline upon termination of the swimming bout (shunted lag) or not (lag).

In contrast, mean interbout duration increased with longer lag only in the non-shunted setting, whereas if the reafference was shunted, increase of the mean interbout duration was not observed (Figure 3.2b). This demonstrates that the duration of a bout and a subsequent interbout can be influenced by the reafference independently. Namely, insufficient reafference in the beginning of the bout, something that is present in both non-shunted and shunted lag settings (black arrows in Figure 2.2b), results in increase of bout duration, whereas excessive reafference after the end of a bout, something that is only present in a non-shunted setting (gray arrow in Figure 2.2b), lengthens the subsequent interbouts.

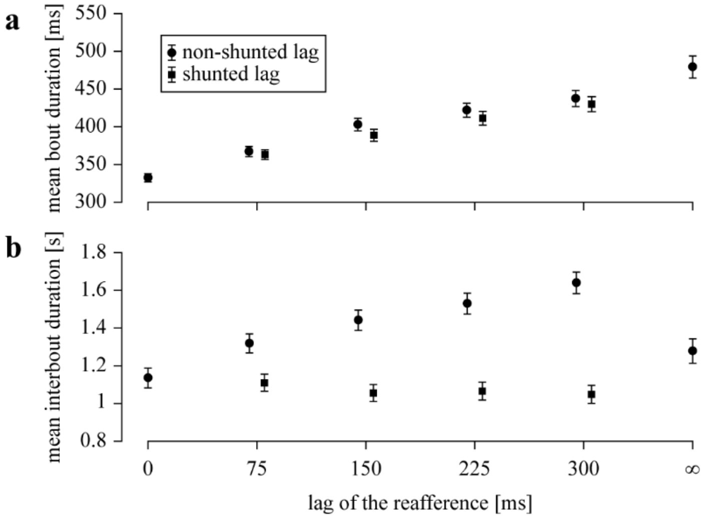

Figure 3.2. Acute OMR adaptation to lag of the reafference

Mean bout duration (**a**) and interbout duration (**b**) as a function of lag of the reafference. Black circles or squares denote the mean values across animals, error bars denote SEM, $N = 100$ larvae. *Figure adapted from Markov et al. (submitted).*

In summary, these results demonstrate that not only the amount of the reafference affects ongoing behavior (Results section 3.1.1), but also the temporal relationship between the behavior and its visual feedback. Furthermore, these results demonstrate that the reafference can influence duration of a bout and a subsequent interbout independently: insufficient reafference during the bout makes it longer, and excessive reafference after the bout prolongs the subsequent interbout.

3.1.3 Acute adaptation to gain drop

To investigate how temporal relationship between the behavior and its visual feedback affects the former in greater detail, I zeroed the gain of the closed loop not during the whole bout, but only during fixed periods of the bout. I refer to this type of reafference perturbation as *gain drop* (Figure 2.2c; Materials and methods section 2.2). The generally observed association of increased bout duration and decreased interbout duration with insufficient reafference during the bout (be it a decreased gain of the closed loop or an increased lag of the reafference) was confirmed and expanded by the analysis of bouts and interbouts as a function of gain drop profile (Figure 3.3). The mean bout duration was prolonged differentially depending on what bout segment had a perturbed reafference. Overall, a segment with a gain of 0 had a larger effect on increasing bout duration the earlier it occurs within the bout: compare for example the cases for gain drop profiles 0111 and 1110 (gray arrowheads in Figure 3.3a). In contrast, interbouts were affected more when the gain was dropped in segments closer to the end of the bout. Taken together, these results demonstrate that the acute effects of the reafference on ongoing behavior dynamically change during the course of the bout. Thus, reafference closer to the beginning of the bout has more influence over duration of that bout and less influence over the subsequent interbout duration than reafference closer to the end of the bout.

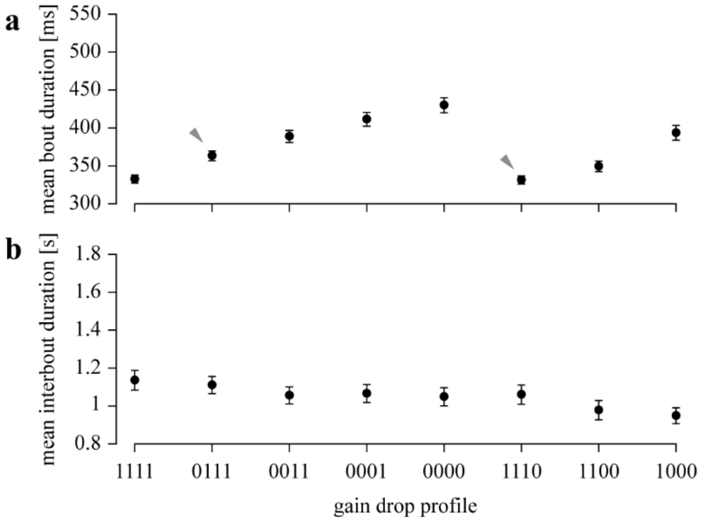

Figure 3.3. Acute OMR adaptation to gain drop

Mean bout duration (**a**) and interbout duration (**b**) as a function of gain drop setting. Gray arrowheads indicate two cases, when the reafference was perturbed for the same duration, but at different time points with respect to the bout onset. Black circles denote the mean values across animals, error bars denote SEM, $N = 100$ larvae. *Figure adapted from Markov et al. (submitted).*

3.1.4 Reaction time delay during acute adaptation

To identify more subtle effects of reafference on ongoing behavior, I focused on the temporal dynamics of the tail beat amplitude within individual bouts in the form of bout power (Materials and methods section 2.3.2). Comparing the mean bout power profiles across different reafference conditions has revealed that if the reafference was different from that of gain 1 from the very beginning of a bout (as in *gain change*, *lag* and *shunted lag* conditions), the mean bout power profile started to deviate only 220 ms after the bout onset (Figure 3.4a-c). However, if the change in the reafference was introduced after the bout had already started (as in the *gain drop* condition with profiles 1000, 1100), the deviation in the respective mean bout power was observed only around 220 ms after the start of the perturbation in reafference (see blue traces in Figure 3.4d). This analysis reveals that larval zebrafish react to changes in visual reafference with a 220 ms delay.

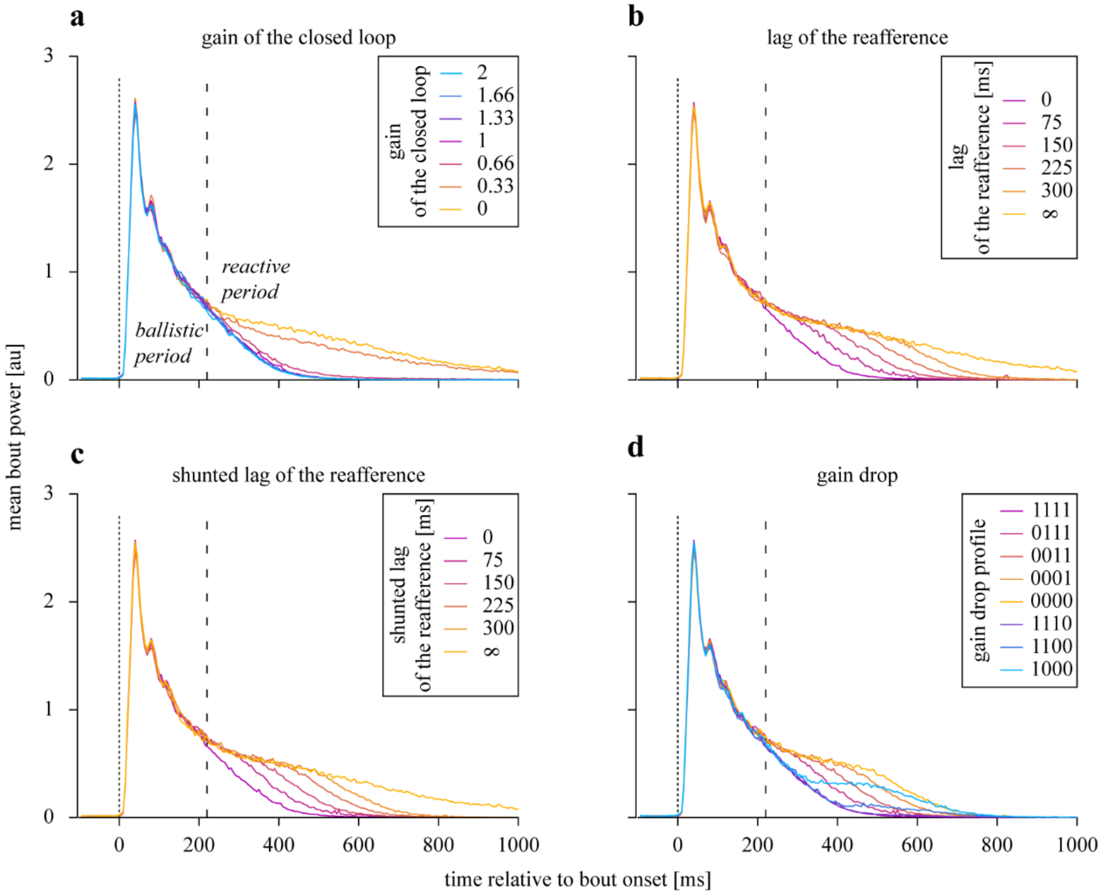

Figure 3.4. Ballistic and reactive periods of swimming bouts

Mean bout power profile as a function of gain of the closed loop (**a**), lag of the reafference (**b**), shunted lag of the reafference (**c**), and gain drop setting (**d**). Dotted lines denote bout onsets, dashed lines separate ballistic and reactive periods from each other. Each line represents the mean bout power profile across animals. Note that bout power during the ballistic period did not depend on the reafference condition. *Figure adapted from Markov et al. (submitted).*

This reaction delay suggests that the bouts can be divided into two well-defined periods: an initial stereotyped ballistic period lasting 220 ms and a subsequent reactive period. A change in reafference condition (regardless of whether this change occurred during the ballistic or the reactive period), can only affect the bout power during the reactive period (Figure 3.5).

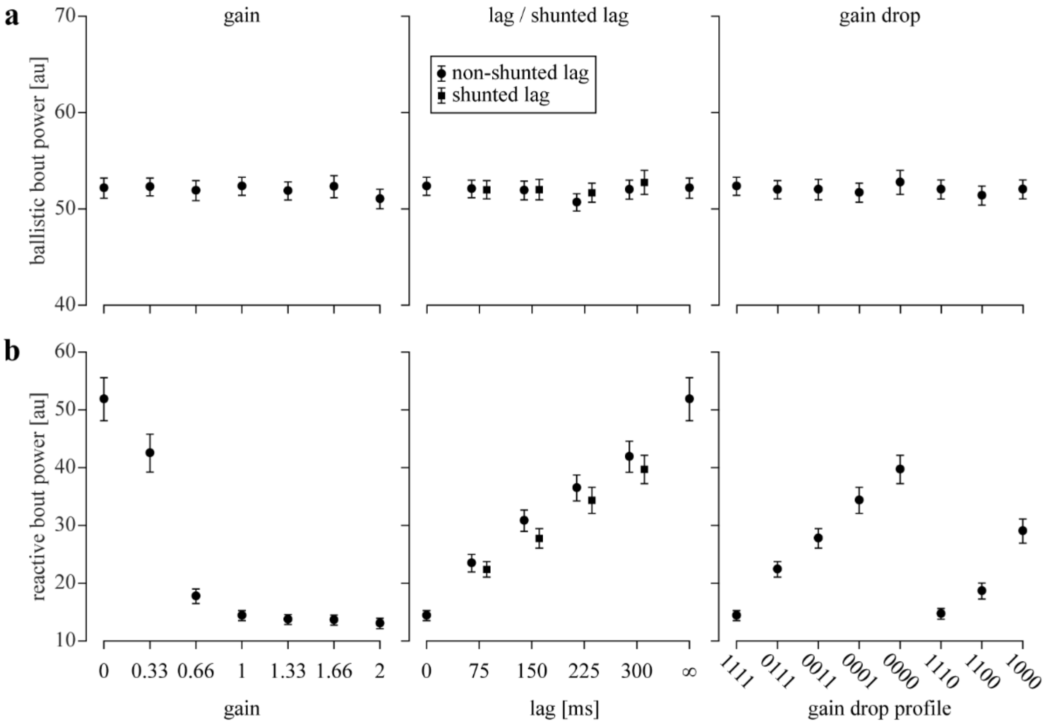

Figure 3.5. Acute adaptation of ballistic and reactive bout power

Area below the bout power curve during the ballistic (**a**) and reactive (**b**) periods of the swimming bouts as a function a reafference condition. Note that the bout power during the reactive, but not ballistic, period depended on the reafference. Black circles and squares denote the mean values across animals, error bars denote SEM, $N = 100$ larvae. *Figure adapted from Markov et al. (submitted).*

3.1.5 Summary

These results demonstrate that larval zebrafish can change their optomotor behavior within a bout depending not only on the absolute amount of reafference that they receive, but also on the temporal relationship between their swimming and its accompanying reafference. In general, the less reafference the larva received during the bout, the more motor output it produced. Analysis of bout power revealed that it takes zebrafish larvae 220 ms to implement any behavioral change, which must encompass delays in sensory processing and implementation of behavioral modifications. This delay suggests that acute OMR adaptation may result from a feedback control mechanism, since feedback controllers are accompanied by sensory processing delays. In addition, this observation allows us to define an initial ballistic period of the bout, which is stereotyped across reafference conditions and can therefore be used as a readout of the state of the controller that performs sensory-motor transformation, i.e. determines how forward motion of the grating is transformed into OMR.

3.2 Involvement of PCs in acute OMR adaptation

Many forms of motor adaptation and learning has been shown in both zebrafish (Ahrens et al., 2012; Aizenberg and Schuman, 2011; Harmon et al., 2017) and other vertebrates (de Zeeuw et al., 1998; Ito, 1982; Raymond et al., 1996) to involve cerebellar circuitry. I therefore aimed to test the involvement of the cerebellum in the acute adaptation of the OMR. To this end, I used a transgenic line *PC:*epNtr-tagRFP (*contribution of Andreas Kist*) that expresses Ntr specifically in all PCs (Materials and methods section 2.1.3).

Treatment of *PC*:epNtr-tagRFP$^+$ fish with MTZ resulted in ablation of PCs one day after treatment. I observed swelling and destruction of the PC nuclei and aggregation of the cell membranes into puncta with complete loss of the characteristic filiform structure (Figure 3.6).

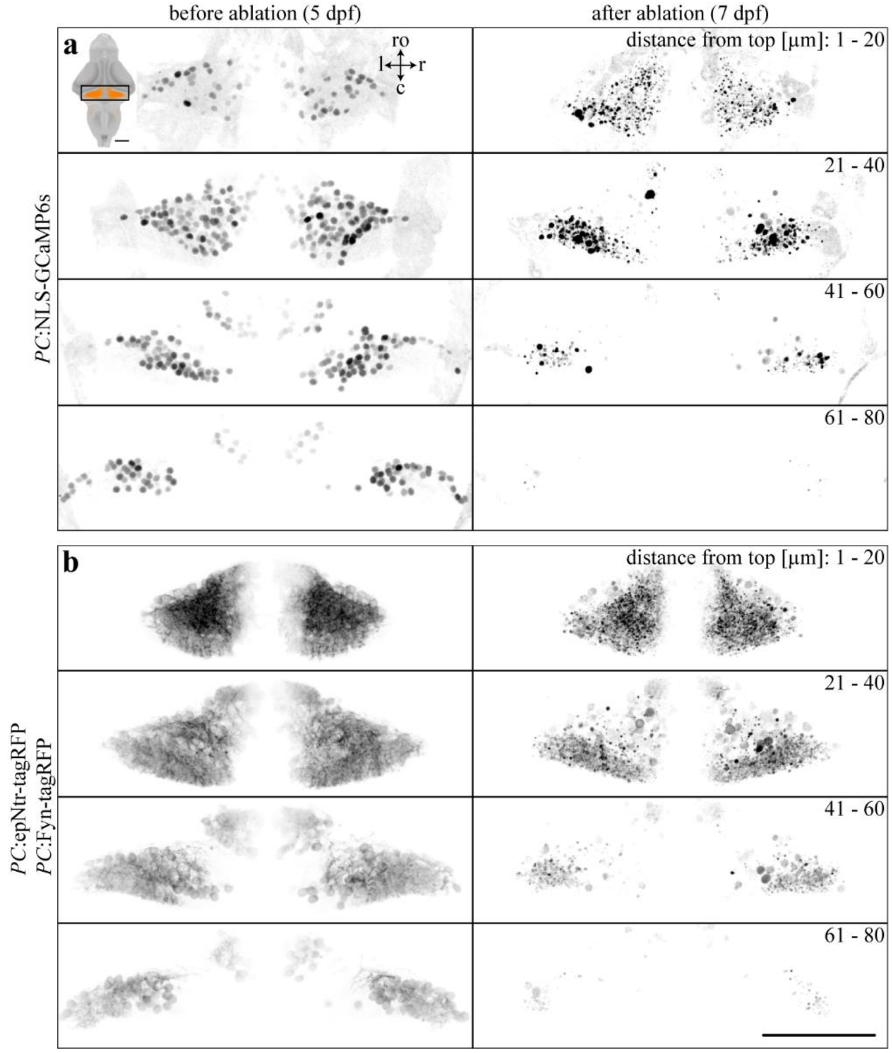
before ablation (5 dpf)
after ablation (7 dpf)
a
ro
l
r
c
distance from top [µm]: 1 - 20
21 - 40
41 - 60
61 - 80
PC:NLS-GCaMP6s
b
distance from top [µm]: 1 - 20
21 - 40
41 - 60
61 - 80
PC:epNtr-tagRFP
PC:Fyn-tagRFP

Figure 3.6. Targeted pharmaco-genetic ablation of PCs

a. PC nuclei-localized GCaMP6s signal before and after PC ablation. Small inset is taken from Figure 1.4b to show the location of the cerebellum within the larval zebrafish brain. **b**. Membrane-tagged RFP signal before and after PC ablation. In both panels, each image is a maximum z-projection of 20 confocal optical slices from an example larva, each 1 µm thick. Scale bar denotes 100 µm.

I tested these PC-ablated larvae in the acute adaptation paradigm (Materials and methods sections 2.2, 2.3.1). After PC ablation, zebrafish larvae were still able to perform OMR, indicating that PCs are not crucial for detection of the forward moving grating and for the behavioral reaction to this stimulus. This is consistent with the fact that destruction of the cerebellum in other animals does not produce paralysis or sensory deficits, indicating that it is not a primary way station of sensory-motor transformation during motor control (Llinás et al., 2004). Interestingly, PC-ablated larvae displayed increased motor activity: a longer mean bout duration than both treatment controls and wildtypes in every single condition and shorter interbouts than those of the treatment control animals (Figure 3.7). This is consistent with the idea that the GABAergic nature of the PCs may provide a tonic inhibitory effect on premotor areas in the brain. In addition, increased motor activity following ablation of the PCs confirms the effectiveness of the ablation protocol.

Surprisingly, ablation of the PCs did not result in any impairment of the larvae’s ability to adapt their behavior acutely to changes in visual reafference: all aspects of acute adaptation were also present in PC-ablated animals (Figure 3.7). This result demonstrates that acute adaptation of OMR, described in the Results section 3.1, is not PC-dependent.

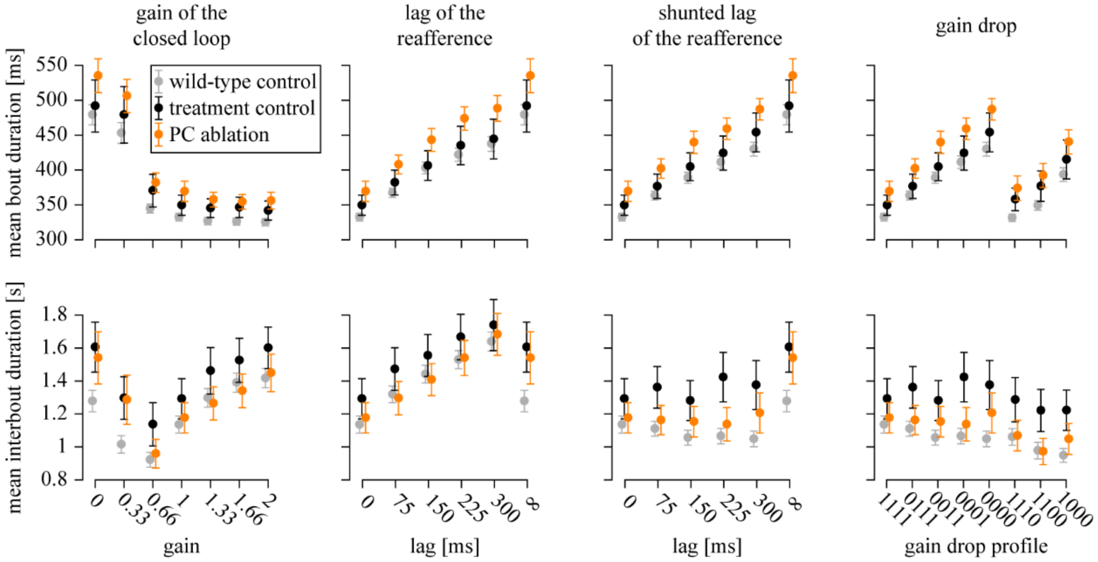

Figure 3.7. Acute OMR adaptation after PC ablation

Mean bout duration (top) and mean interbout duration (bottom) as a function of reafference condition in wild-type control animals (gray, *N* = 100 larvae, data repeated from Figure 3.1 – Figure 3.3), treatment control animals (black, *N* = 28 larvae) and PC-ablated animals (orange, *N* = 39 larvae). Circles denote the mean values across animals, error bars denote SEM. Note that mean bout duration was longer and interbout duration was shorter in PC-ablated animals compared to the treatment control group, and that PC-ablated animals can acutely adapt their behavior to changes in reafference despite the ablation. *Figure adapted from Markov et al. (submitted).*

3.3 Feedback control model of acute OMR adaptation

3.3.1 Design and behavior of the model

Given that the observed acute adaptation is only implemented after a relatively long initial ballistic period of 220 ms (Results section 3.1.4; Figure 3.4, Figure 3.5) and that it is not PC-dependent (Results section 3.2; Figure 3.7), I hypothesized that the acute adaptation is implemented by a feedback controller. This idea contrasts with previously proposed forward model-based hypothesis that suggests that larval zebrafish have an internal representation of expected reafference, compare this expectation with actually observed reafference, and adapt their behavior if there is a mismatch (Introduction section 1.3.2, also see discussion in Portugues and Engert, 2011). Explicitly, a feedback controller measures a particular variable of a system and generates an output that tries to keep this variable at a given value (see Introduction section 1.1.1 for further details). In the case of OMR, when fish swim in a closed-loop assay, the grating slows down with respect to the fish, so it is natural to postulate that the aim of the controller is to minimize the forward motion of the visual stimulus so that fish will swim as long as the grating is moving forward. I therefore defined such a feedback controller and tested its performance under the acute adaptation experimental paradigm.

The designed feedback controller is rather simple (Figure 3.8a). It is based on the assumption that the motor output of larval zebrafish during OMR depends on the level of *sensory drive*, defined as forward motion of the grating integrated in time. If the grating moves forward, the sensory drive accumulates, and at some point reaches a motor command threshold resulting in initiation of a swimming bout. If the animal receives visual reafference (i.e. grating decelerates), the level of sensory drive goes down, and the bout stops. The core idea of the model is that insufficient reafference results in increased motor output *not because* it does not match the putative internal expectation, *but because* it is accompanied by increased sensory drive (i.e. grating moves forward faster / longer during a bout with less reafference). More explicitly, the information flow within the model starts in a sensory part that instantaneously combines the forward and backward grating velocity with excitatory and inhibitory weights, respectively, and integrates this forward drive in time in a SI (see Figure 3.8a for abbreviations). This sensory drive computed by the SI is then fed forward to a MOG, which generates a motor output command whenever its activity reaches a threshold. As larvae swim in discrete bouts, I added a MI that inhibits the MOG and will eventually result in the termination of the bout, although only after the self-excitation within the motor output is overcome (see Materials and methods section 2.4.1 for further details).

With a certain combination of parameters, the model was able to produce bouts and interbouts with realistic duration (Figure 3.8b, green trace). It can be noted in the panel that bout and interbout duration differed depending on the reafference condition, similarly to acute adaptation in real larvae. Thus, for example, a bout performed at open loop (bout # 2) is longer than a closed-loop bout (bout # 1), or interbout following a bout with non-shunted lag of the reafference (bout # 5) is longer than that with the shunted lag (bout # 6).

I was able to optimize parameters of the model (Materials and methods section 2.4.2) so that its behavior closely reproduced the main findings of the acute adaptation experiment (Figure 3.9). This allowed me to conclude that the observed acute adaptation of the OMR to changes in visual reafference may indeed be implemented by a simple feedback controller that relies on integration of the sensory evidence of the forward moving stimulus in time and does not necessarily involve internal representation of expected reafference.

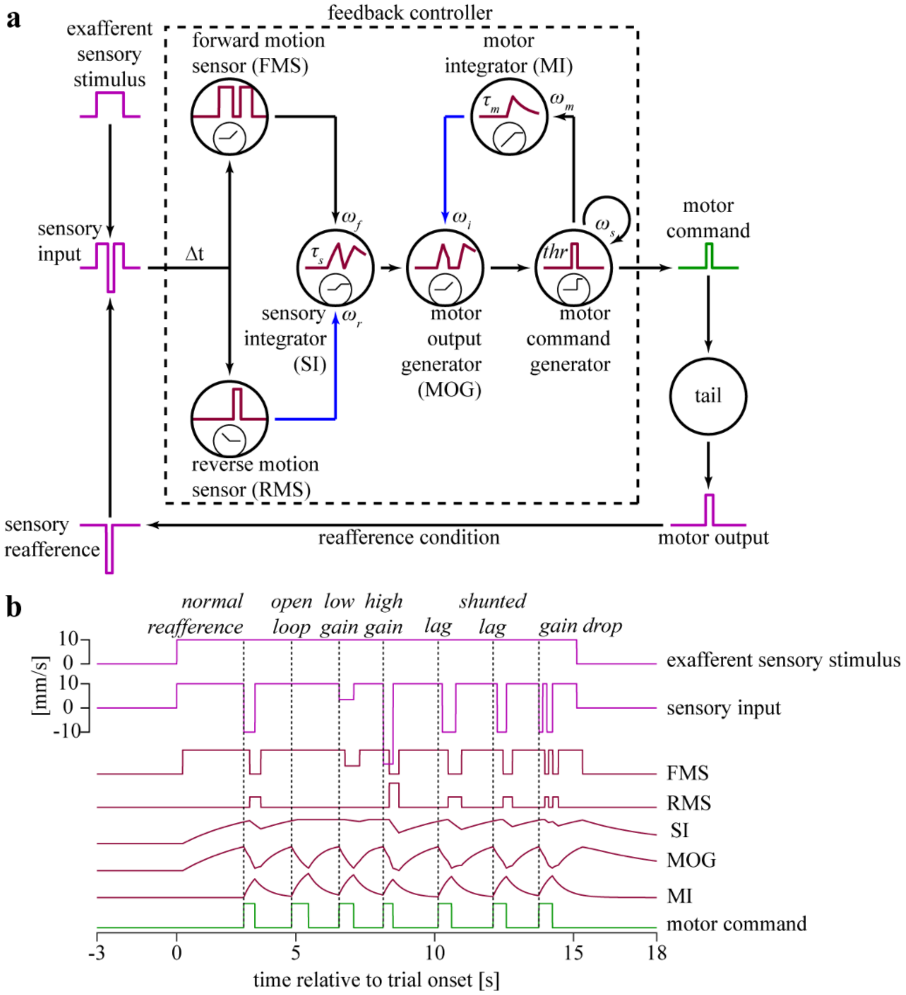
a
feedback controller
exafferent sensory stimulus
forward motion sensor (FMS)
motor integrator (MI)
τ_m
ω_m
ω_f
ω_i
ω_s
sensory input
Δt
τ_s
thr
motor command
sensory integrator (SI)
ω_r
motor output generator (MOG)
motor command generator
tail
reverse motion sensor (RMS)
sensory reafference
reafference condition
motor output
b
normal reafference
open loop
low gain
high gain
lag
shunted lag
gain drop
[mm/s]
10
0
10
0
-10
exafferent sensory stimulus
sensory input
FMS
RMS
SI
MOG
MI
motor command
-3
0
5
10
15
18
time relative to trial onset [s]

Figure 3.8. Feedback controller of acute adaptation

a. Schematic diagram of the model. Blue lines indicate inhibitory connections. Black circles depict the model nodes, small black circles inside the nodes depict schematic pictograms of nonlinear transformations performed by respective nodes. Italic letters indicate parameters of the model; Δt denotes the sensory processing delay of 220 ms. **b**. Example trial demonstrating the behavior of the model. Dotted lines denote bout onsets. See further details in the text of this section, and Materials and methods section 2.4.1. *Figure adapted from Markov et al. (submitted).*

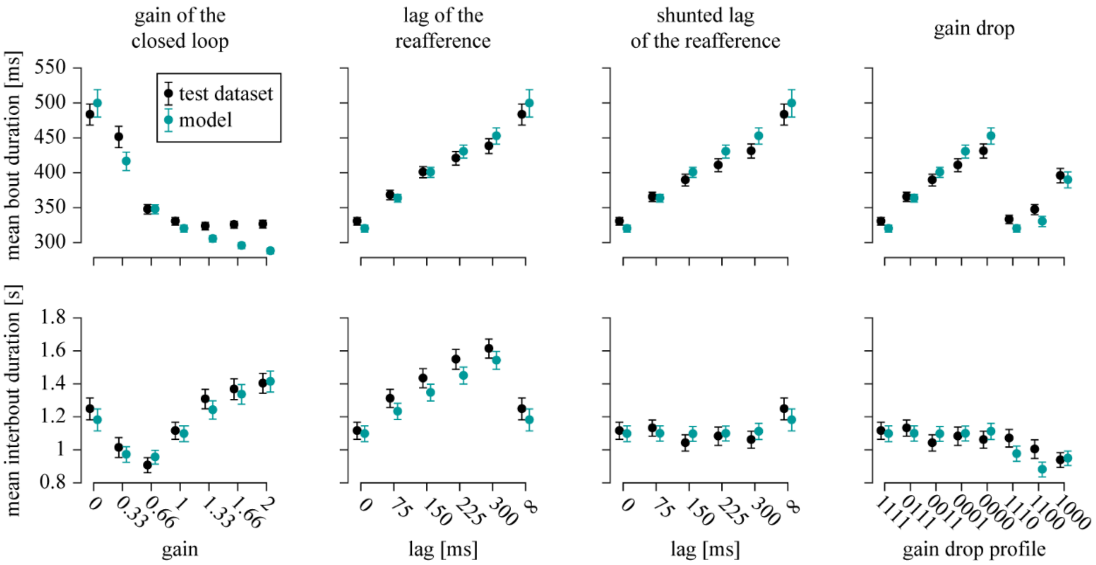

Figure 3.9. Acute adaptation of the feedback control model

Mean bout duration (top) and mean interbout duration (bottom) as a function of reafference condition in the test dataset (a subset of the data presented in Results section 3.1, that was never used for training the models, denoted by the black color, N = 100 larvae) and in the feedback control models, each optimized to fit one larva from the training dataset (denoted by the cyan color). Circles denote the mean values across animals, error bars denote SEM. *Figure adapted from Markov et al. (submitted).*

3.3.2 Sensory integration in the larval zebrafish brain

(contribution of Luigi Petrucco)

To test the main assumption of the model: the existence of the sensory integration in the larval zebrafish brain, we performed whole-brain, light sheet functional imaging experiments in head-restrained behaving larvae (Materials and methods section 2.5).

After segmenting the imaged brains into ROIs, I first aimed to identify ROIs with reliable responses to the moving grating, in order to subsequently determine whether some of these ROIs exhibit properties of SIs. Since trials of moving grating were often accompanied with the OMR, it was important to disambiguate ROIs with sensory responses from motor-related ROIs. To this end, I analyzed mean fluorescence triggered by grating and bout onsets (Materials and methods section 2.5.3). I observed ROIs that increased their fluorescence at the onset of the moving grating (sensory ROIs) or when the larvae were performing bouts (motor ROIs). Figure 3.10a demonstrates activity of two example ROIs in one trial, displaying sensory or motor-related activity (their location within the reference larval zebrafish brain is presented in Figure 3.10b). It can be noted that the sensory ROI increased its fluorescence in response to the stimulus onset before the first bout was initiated, whereas the motor ROI did not respond to the stimulus, and increased its fluorescence only after the larva started swimming (Figure 3.10a, c). Analysis of the mean fluorescence triggered by grating movement or bout onset revealed that sensory and motor ROIs accounted for a significant fraction of the total number of ROIs (respectively, 32 ± 3 % and 30 ± 5 %, mean ± SEM across animals; mean triggered activity of all sensory and motor ROIs is presented in Figure 3.10d). Motor ROIs were located predominantly in the hindbrain, whereas sensory ROIs mostly occupied hindbrain, midbrain and diencephalic regions, including IO, DRN, OT, preT, and Thal (Figure 3.10e, see also Figure 2.3c for anatomical annotation).

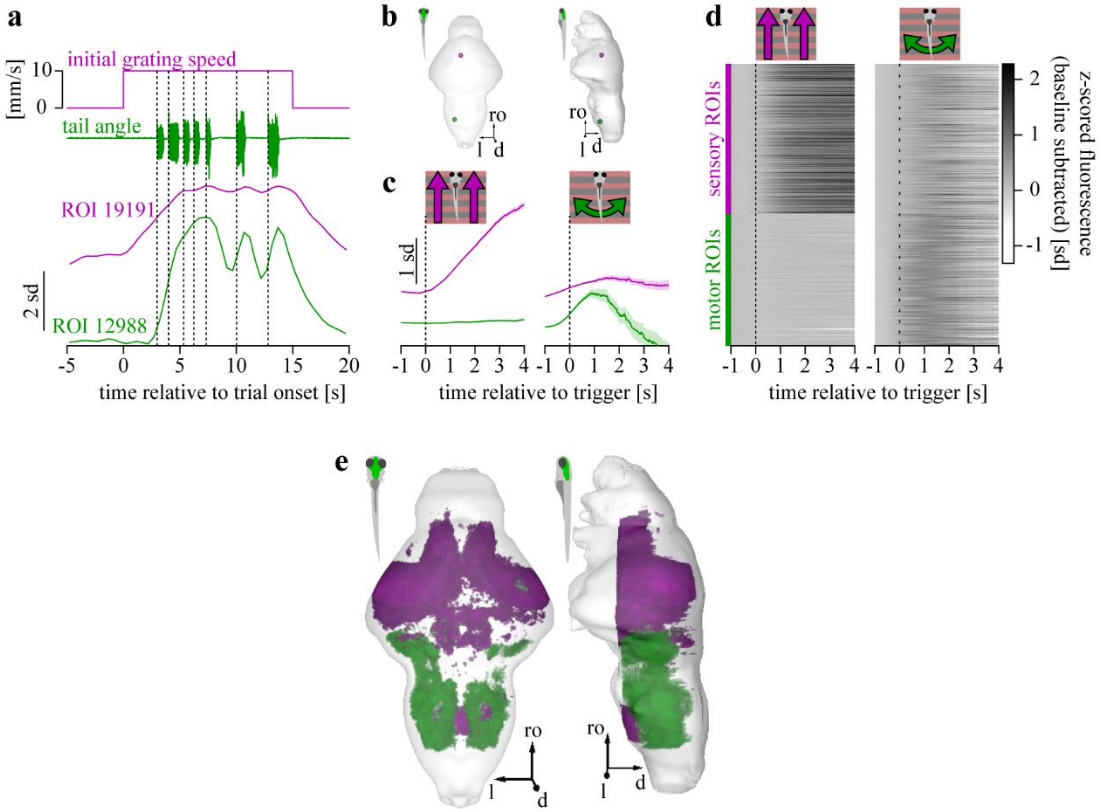

Figure 3.10. Sensory and motor ROIs in the larval zebrafish brain

a. Example trial illustrating fluorescence traces of a sensory (magenta) and a motor (green) example ROIs. Dotted lines denote bout onsets. **b**. Location of the example ROIs presented in **a** within the reference brain; ro – rostral direction, d – dorsal, l – left; the length of the scale arrows is 100 µm. **c**. Mean grating- and bout-triggered fluorescence, of the example ROIs presented in **a,** averaged across all triggers. Shaded areas denote SEM. In **c** and **d**, dotted lines denote triggers (grating or bout onsets). **d**. Mean grating- and bout-triggered fluorescence of all sensory and motor ROIs pooled from all imaged larvae ($N = 4$ larvae). **e**. Location of all sensory and motor ROIs within the reference brain. *Figure adapted from Markov et al. (submitted).*

I then focused on sensory ROIs and discovered that the fluorescence rise-time after grating onset varied greatly across these ROIs. Figure 3.11a demonstrates activity of two example sensory ROIs with fast or slow fluorescence rise after the grating onset (their location within the reference brain is presented in Figure 3.11b). To identify whether some of the sensory ROIs integrate sensory evidence in time, I fitted a leaky integrator model to the mean grating-triggered fluorescence of each of these ROIs (two examples are presented in Figure 3.11c). Resulting leaky integration time constant was zero for the majority of sensory ROIs (73 ± 4 %, mean ± SEM.), indicating that these ROIs do not integrate sensory evidence and could be therefore termed *sensors*, as opposed to the remaining 27 ± 4 % sensory ROIs with non-zero time constants which were called *integrators*. 95 % of the integrators' time constants fall between 0.1 and 0.9 seconds, with the mean value 0.31 ± 0.05 seconds (mean ± SEM across animals; Figure 3.11f). Mean grating-triggered activity of all sensors and integrators is presented in Figure 3.11d, and the traces averaged across ROIs within each larva and then across larvae are presented in Figure 3.11e. Sensors and integrators occupied distinct brain regions: sensors were located predominantly in the OT and the IO, whereas DRN and diencephalic regions including Thal and preT were occupied by the integrators (Figure 3.11g, see also Figure 2.3c for anatomical annotation).

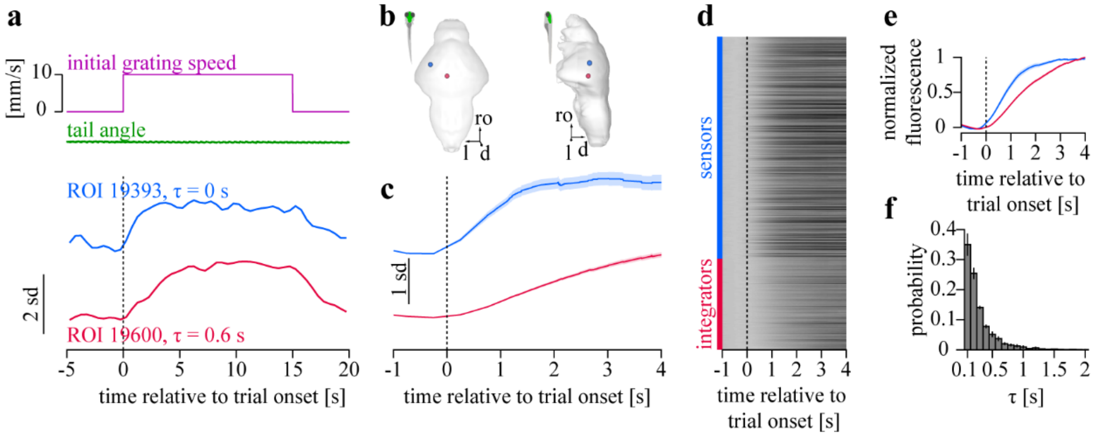

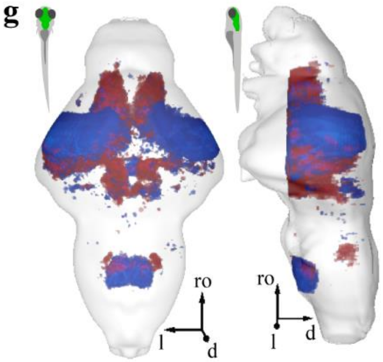

Figure 3.11. Sensory integration in the larval zebrafish brain

a. Example trial illustrating fluorescence traces of two example sensory ROIs with fast (blue) and slow (red) fluorescence rise after the grating onset (denoted by dotted lines). The trial without swimming (green trace) was chosen to illustrate that fluorescence rise time is not related to behavior and rather reflects sensory processing. **b**. Location of the example ROIs presented in **a** within the reference brain; ro – rostral direction, d – dorsal, l – left; the length of the scale arrows is 100 µm. **c**. Mean grating-triggered fluorescence of the example ROIs presented in **a,** averaged across trials. Shaded areas denote SEM. **d**. Mean grating-triggered fluorescence of all sensory ROIs, separated into sensors and integrators, from all imaged larvae ($N = 4$ larvae). **e**. Mean grating-triggered fluorescence of sensors and integrators, first averaged across ROIs within each animal, and then across animals. Shaded areas denote SEM across animals. The traces were scaled to range from 0 to 1 to illustrate different rise times. **f**. Distribution of time constants across sensory ROIs, vertical lines denote SEM across animals. **g**. Location of all sensors and integrators within the reference brain. *Figure adapted from Markov et al. (submitted).*

Therefore, certain regions of the larval zebrafish brain (namely the DRN, preT, and Thal) integrate sensory evidence in time, consistent with recent findings using different behavioral paradigms (Dragomir et al., 2019, Bahl and Engert, 2019). This provides an important substrate for the feedback control mechanism of acute adaptation.

3.4 Long-term OMR adaptation

After concluding that the mechanism of acute adaptation is not cerebellum-dependent and could presumably be implemented by a feedback controller, I aimed to test whether zebrafish larvae could perform long-term motor adaptation and whether this adaptation is cerebellum-dependent.

To this end, zebrafish larvae were exposed to a consistent long-term perturbation in reafference condition, namely, to 225 ms lag (Materials and methods sections 2.2 and 2.3). As expected from the results of acute adaptation experiments, animals adapted to this lag by increasing the bout duration (Figure 3.12a). However, the first bout duration gradually decreased throughout the adaptation session, reached the pre-adaptation level by the end of the session, and became statistically indistinguishable from the control group that was never exposed to lagged reafference (normal-reafference control group) (Figure 3.12a, b). In addition, when normal reafference was reinstated after the adaptation session, the lag-trained animals demonstrated a significant after-effect of decreased bout duration compared to the normal-reafference control animals (Figure 3.12a, c). These results demonstrate that exposure to a perturbed reafference condition for a prolonged time leads to long-term recalibration of bout duration in the direction that diminishes the effects of acute adaptation.

As reported above (Results section 3.1.4), bout power during the ballistic period does not depend on the reafference condition but reflects the state of the neuronal controller that converts the sensory information about the moving grating into OMR. Therefore, any change in the ballistic power would automatically reflect a change in the controller. Analysis of changes in first bout power profiles from trial to trial revealed that bout power during the ballistic period gradually increased throughout the experiment (Figure 3.13a). This increase did not depend on whether animals were exposed to lag or to normal reafference during the adaptation session (Figure 3.13b).

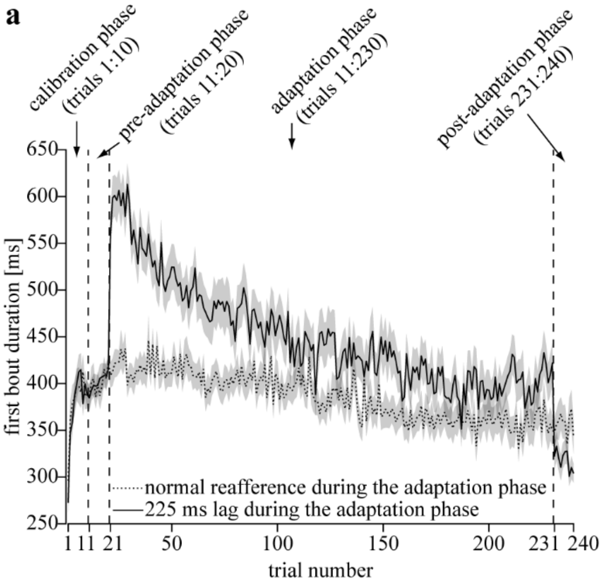

Figure 3.12. Changes in first bout duration during long-term OMR adaptation

a. Changes of first bout duration in normal reafference control (solid line, N = 103 larvae) and lag-trained animals (dotted line, N = 100 larvae) from trial to trial, averaged across animals. Shaded areas denote SEM. Vertical dashed lines separate the 4 phases of the long-term adaptation experimental paradigm: calibration phase, pre-adaptation phase, adaptation phase and post-adaptation phase (Materials and methods section 2.3.1). **b**. Change of first bout duration in the last 10 adaptation trials with respect to the pre-adaptation trials (first averaged across 10 trials, and then across animals). Black circles denote the mean values across animals, vertical lines denote the SEM; n.s. - p > 0.05, * - p < 0.05 (Mann-Whitney U test). **c**. Long-term adaptation after-effect measured as change of the first bout duration in the post-adaptation trials with respect to the pre-adaptation trials. *Figure adapted from Markov et al. (submitted).*

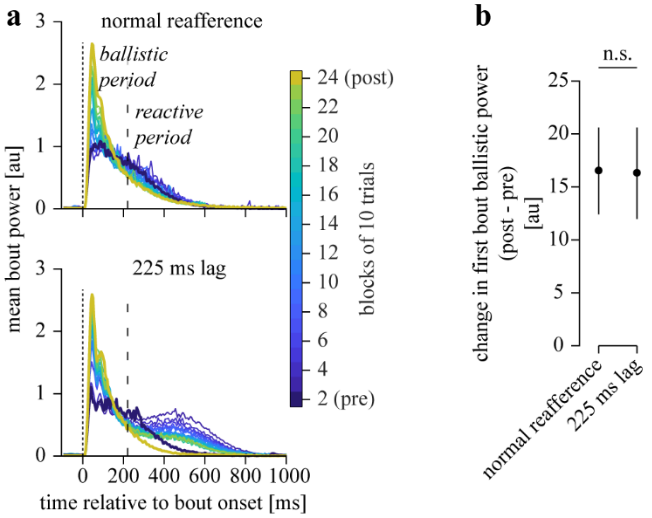

Figure 3.13. Changes in first bout power during long-term OMR adaptation

a. Changes in first bout power of normal-reafference control (top, $N = 103$ larvae) and lag-trained animals (bottom, $N = 100$ larvae) from trial to trial. Each trace is first bout power, averaged across 10 trials and then across animals. Dotted lines denote first bout onsets, dashed lines separate ballistic and reactive periods from each other. Note that the first bout power during the ballistic period increased during the course of the experiment. **b**. Increase in first bout ballistic power in the post-adaptation phase with respect to the pre-adaptation phase. Ballistic power was quantified as area below the bout power curves within the ballistic period, first averaged across 10 trials, and then across animals. Black circles denote the mean values across animals, vertical lines denote SEM; n.s. - $p > 0.05$ (Mann-Whitney U test). *Figure adapted from Markov et al. (submitted).*

Presented results suggest that larval zebrafish are able to recalibrate the parameters of the controller underlying the sensorimotor transformation during optomotor behavior. This recalibration is reflected in three ways. Firstly, there is a decrease of acute adaptation of first bout duration by the end of the long-term adaptation to lag (Figure 3.12a, b). Secondly, there is an after-effect of decreased first bout duration during the post-adaptation phase in lag-trained animals compared to the normal-reafference control (Figure 3.12a, c). Thirdly, there is an increase in first bout power during the ballistic period after the long-term adaptation in both lag-trained and normal-reafference control groups (Figure 3.13).

3.5 Involvement of PCs in long-term OMR adaptation

To test whether the recalibration of the internal OMR controller is cerebellum-dependent, I conducted long-term adaptation experiments in PC-ablated animals (Materials and methods section 2.1.3), and analyzed the three parameters that reflect the recalibration of the controller (Results section 3.4).

Firstly, I observed that by the end of the adaptation session, lag-trained PC-ablated animals did not decrease their first bout duration to the pre-adaptation level and maintained high motor activity throughout the whole adaptation session (Figure 3.14a). Secondly, the after-effect of decreased bout duration during the post-adaptation phase in lag-trained animals was also absent after PC-ablation. However, this effect was also diminished in the treatment control group, indicating that it could possibly result not only from the PC ablation itself but also from treatment with MTZ (Figure 3.14b). Finally, the increase in bout power during the ballistic period was also significantly less prominent in PC-ablated animals (Figure 3.14c). Taken together, these results demonstrate that long-term recalibration of the internal OMR controller is cerebellum-dependent.

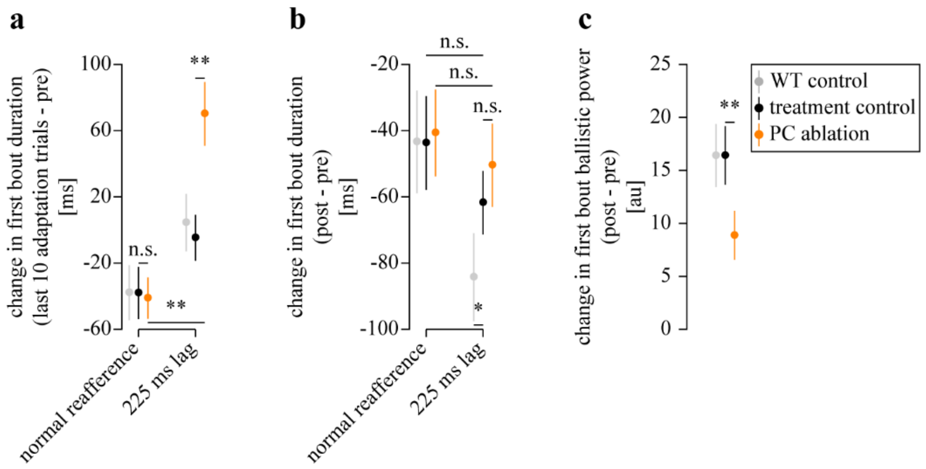

Figure 3.14. Long-term OMR adaptation after PC ablation

a. Change of first bout duration in the last 10 adaptation trials with respect to the pre-adaptation trials (similar to Figure 3.12b). **b**. Long-term adaptation after-effect (similar to Figure 3.12c). **c**. Increase in first bout ballistic power in the post-adaptation phase with respect to the pre-adaptation phase (similar to Figure 3.14b). Gray color represents wild-type control animals (*N* = 103 and 100 larvae for normal-reafference control and lag-trained groups, respectively; data repeated from Figure 3.12 and Figure 3.13); black color represents treatment control animals (*N* = 85 and 85 larvae); orange color represents PC-ablated animals (*N* = 83 and 90 larvae). Circles denote the mean values across animals, vertical lines denote SEM; n.s. - p > 0.05, * - p < 0.05, ** - p < 0.01 (Mann-Whitney U test). *Figure adapted from Markov et al. (submitted).*

4. Discussion

4.1 Feedback control mechanism of acute OMR adaptation

The present study demonstrates that larval zebrafish change their behavior within a swimming bout depending on the visual feedback they receive during that bout, and that these acute within bout changes are not cerebellum-dependent. Furthermore, by using a variety of sensory perturbations, I show that larvae require at least 220 ms to implement these behavioral changes, even if the sensory feedback was only altered during the initial 75 ms of the swimming bout. This delay is consistent with previously reported delays involved in processing of feedback visual signals and implementing resulting behavioral adjustments (Barnett-Cowan and Harris, 2009; Brenner and Smeets, 2003; Desmurget and Grafton, 2000; Saunders and Knill, 2003; Saunders and Knill, 2005).

Previous studies proposed that larval zebrafish use forward internal models during acute OMR adaptation (Ahrens et al., 2012; Portugues and Engert, 2011). The forward models can predict expected sensory feedback based on what motor action the animal is about to perform. If the predicted feedback does not match the actually observed feedback, behavior needs to be adjusted, and an error signal can be generated to drive changes in the neuronal circuit underlying the OMR. Furthermore, forward modelling and computation of the error signal were proposed to involve the olivo-cerebellar system.

In contrast, the feedback processing delay and cerebellar-independence of acute OMR adaptation observed in the present study, suggest that this phenomenon can rather be understood in terms of a feedback control mechanism. To support this hypothesis, I present a *rigid* and *simple* feedback controller that implements all experimentally observed acute behavioral adaptations. The controller is *rigid* in a sense that it can produce different motor outputs without changing its intrinsic parameters, and *simple* in a sense that it does not rely on any internal modelling. However, it is important to note here that the long-term adaptation experiments demonstrate that under certain conditions, intrinsic parameters of the controller can be changed, and I show that *this* process relies on cerebellar output (see more details below).

The sensory part of the proposed feedback controller starts with direction-selective sensors whose output is integrated in time by a SI, and the output of the SI drives activity in the motor part of the controller. Direction-selectivity can be observed in the brain already at the level of retinal ganglion cells in vertebrates (Barlow and Hill, 1963; Barlow et al., 1964), including zebrafish larvae (Gabriel et al., 2012; Nikolaou et al., 2012). Presented functional imaging experiments revealed that the sensory integration of the forward visual motion indeed takes place in several brain regions including the preT (Figure 3.11g). Consistent with the architecture of the proposed model, where the SI receives input from direction-selective sensors, the preT receives projections from the contralateral direction-selective retinal ganglion cells (Burrill and Easter, 1994; Gamlin, 2006; Naumann et al., 2016).

An increasing body of evidence highlights the important role of the preT in whole-field visual processing and visuomotor behaviors in larval zebrafish (Kubo et al., 2014; Naumann et al., 2016; Portugues et al., 2014; Severi et al., 2014). Naumann et al. (2016) showed that preT neurons integrate monocular direction-selective inputs from the two eyes and drive activity in the premotor hindbrain and midbrain areas during optomotor behavior. The present study provides evidence that the preT is involved not only in the binocular integration of sensory inputs, but also in temporal integration that underlies accumulation of sensory evidence. Temporal integration in the preT has been recently demonstrated in two other studies where larval zebrafish was presented with sideward visual motion (Dragomir et al., 2019, Bahl and Engert, 2019). In essence, I suggest that the output of the preT can be interpreted as the sensory drive, which is accumulated over time and is subsequently fed to the downstream premotor circuits.

4.2 Long-term cerebellar effects on the feedback controller

Results of the long-term adaptation experiment demonstrate that when the reafference is perturbed consistently over a prolonged period of time, zebrafish larvae gradually adapt their behavior. Furthermore, in contrast with the acute OMR adaptation, these long-term changes are cerebellum-dependent. This suggests that the cerebellum is required to implement this gradual adaptation to a consistent, long-term change in reafference and may therefore recalibrate the parameters of the controller underlying the OMR.

The fact that the cerebellum is required to change a motor program in the long-term is consistent with its role in predictive processing. In the acute bout-by-bout adaptation, the reafference conditions change constantly so no pattern can be learned and predicted. However, if the reafference condition is perturbed consistently, the cerebellum does play a role. This suggests that during the acute adaptation, perturbations in reafference may be driving the circuitry away from a stable state, and that the action of the cerebellum may be to stabilize this change, for example by homeostatic means (Dietrich and Straka, 2016). In this scenario, a change in reafference during optomotor behavior results in an increase in locomotor output in a cerebellum-independent way, and the cerebellum would act on this circuitry to bring it back to a new stable homeostatic state.

The notion that cerebellum is not involved in online corrections of the movements in response to wrong sensory feedback, but is involved in learning new relations between movements and their feedback in the long-term, is present in other studies on cerebellar function. In two such studies (Izawa et al., 2012; Yavari et al., 2016, see also Introduction section 1.2.2 for more details), humans with impaired cerebellar function and control subjects were both able to update the motor program during a reaching task after the feedback of their movements was altered by the experimenters. However, only control subjects were able to update their feedback estimation after the adaptation session, indicating that the cerebellum is involved in acquiring and updating forward internal models. In the case of long-term OMR adaptation presented in this thesis, a similar process might have taken place. During long-term adaptation to consistently perturbed reafference, animals were observing that their motor commands lead to a novel visual feedback. Eventually, animals with intact cerebella might have recalibrated their forward models in the cerebellum to update their expectation thus making them adequate to the new environmental conditions.

Supposition that the cerebellum in larval zebrafish performing adaptive OMR acts as a forward models helps to interpret increased overall motor activity in PC-ablated animals (Results section 3.2) in the context of state estimation. If we assume that larvae perform swimming bouts in order to reach a desired sensory state (defined as some kinematic parameter, such as desired position or velocity), the question naturally arises of how do the larvae estimate their state. State estimation can be achieved using sensory feedback information, predictive forward modeling, or their combination. A study in humans has shown that if subjects are forced to rely solely on feedback sensory information by perturbing their cerebellar activity, their state estimation lags behind the real state due to slow processing of sensory feedback (Miall et al., 2007, see also Introduction section 1.2.2 for more details). As a result, the motor programs of their movements are computed based on out-of-date sensory information, and the performance in a reaching task drops. If larval zebrafish estimate their position during a swimming bout using not only sensory information, but also predictive forward modelling in the cerebellum, disrupting the cerebellar function will lead to lagged state estimation, so that by the time when they reach the desired position, they would still not “know” it and continue swimming. As a result, the bouts in PC-ablated larvae will be longer, similarly to the notorious hypermetria during goal-oriented movements in cerebellar patients.

Another fact that strongly suggests that the cerebellum in larval zebrafish acts as a forward model during OMR is that, in the present study, IO displayed sensory-related activity (Figure 3.11g). The highly sensory nature of PCs’ complex spikes, that directly result from

IO activity (Eccles et al., 1966), was also reported recently (Knogler et al., 2019). IO activity is believed to convey a teaching signal to the PCs (Albus, 1971; Marr, 1969), that updates the internal models in the cerebellum (Imamizu et al., 2003; Kawato et al., 1987) by modifying synaptic weights in the cerebellar circuitry (Ito et al., 1982; Tabata and Kano, 2009). Since the teaching signal must be expressed in the same coordinates as the output of the internal model (Figure 1.2, Introduction section 1.1.2), sensory nature of the teaching signal indicates that the cerebellar internal model involved in adaptive OMR is forward.

4.3 Concluding remarks, limitations and future directions

In summary, this study demonstrates that acute OMR adaptation to changes in visual reafference can be implemented by a feedback control mechanism, whose intrinsic parameters can be modified by the cerebellar output during long-term adaptation (Figure 4.1a). The proposed feedback controller relies on temporal integration of direction-selective sensory signals. I suggest that output of the SI should be interpreted as the sensory drive that is fed to the downstream premotor circuits. Furthermore, I suggest that the cerebellum in larval zebrafish acts as forward model that monitors efference copies of motor commands and the resulting sensory consequences of these commands (indicated by a wavy line in Figure 4.1a). Eventually, such model learns a motor-to-sensory transfer function and is able to predict sensory feedback from the motor commands.

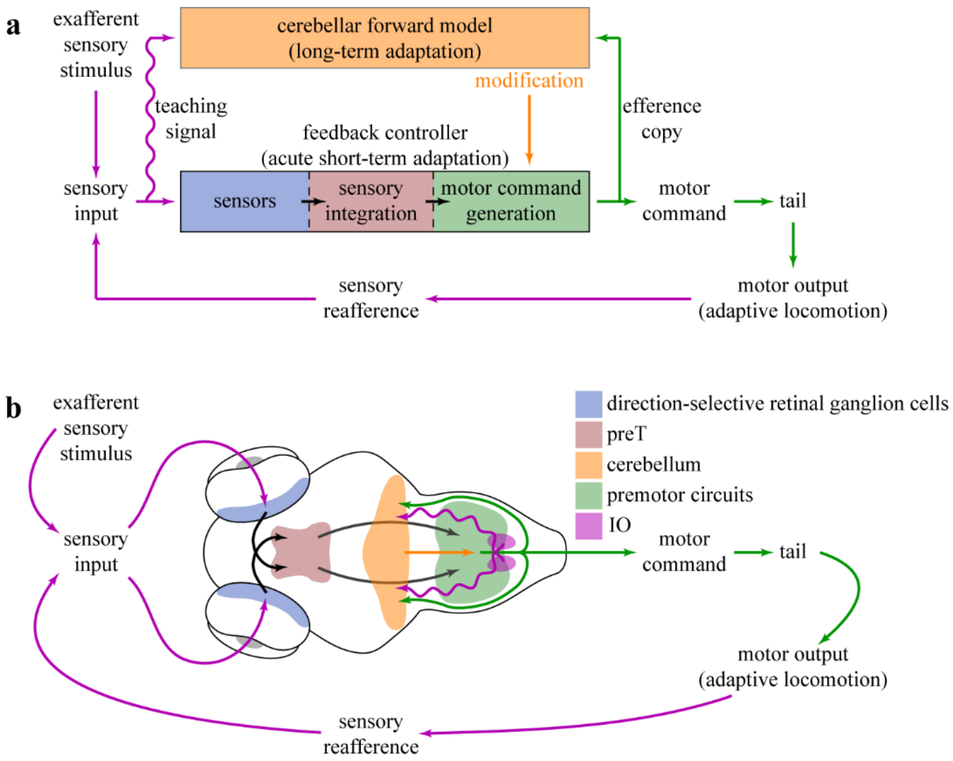
a
exafferent sensory stimulus
cerebellar forward model
(long-term adaptation)
modification
teaching signal
efference copy
feedback controller
(acute short-term adaptation)
sensory input
sensors
sensory integration
motor command generation
motor command
tail
motor output
(adaptive locomotion)
sensory reafference
b
exafferent sensory stimulus
direction-selective retinal ganglion cells
preT
cerebellum
premotor circuits
IO
sensory input
motor command
tail
motor output
(adaptive locomotion)
sensory reafference

Figure 4.1. Proposed mechanism of acute and long-term OMR adaptation

a. Schematic diagram of the feedback controller that can implement acute OMR adaptation to changes in sensory reafference. Cerebellar forward model monitors the efference copies of motor commands and resulting sensory consequences and learns their transfer function. It influences the intrinsic parameters of the controller, presumably, of its motor part. Like in Figure 1.2, wavy line denotes the teaching signal used by the forward model to learn the transfer function. **b**. Mapping of the crucial functional nodes involved in OMR adaptation onto the larval zebrafish brain. See details in text of the Discussion. *Figure adapted from Markov et al. (submitted).*

Based on the functional imaging results presented in this thesis, combined with anatomical and functional literature, the proposed mechanism of acute and long-term OMR adaptation can be mapped, to a certain extent, onto the larval zebrafish brain (Figure 4.1b).

Thus, the central node of the feedback controller – the SI – may correspond to the preT for three main reasons. Firstly, the preT receives direction-selective signals from retinal ganglion cells (Barlow and Hill, 1963; Barlow et al., 1964; Gabriel et al., 2012; Nikolaou et al., 2012). Secondly, presented functional imaging results revealed temporal integration of sensory information in this brain area (Figure 3.11). Finally, the preT drives activity in premotor circuits, and ablation of inputs to the preT impair the OMR, suggesting its crucial role in this behavior (Naumann et al., 2016; Severi et al., 2014).

Regarding long-term adaptation, recent studies have revealed that the cerebellum in larval zebrafish receives both sensory information and efference copies of motor commands (Knogler et al., 2017), which is necessary for acquiring and updating an internal model. Furthermore, the present study together with Knogler et al. (2019) demonstrates that IO provides predominantly sensory teaching signals to the PCs (Figure 3.10), suggesting that the cerebellum acts as a forward model. Given that the zebrafish cerebellum projects to a wide range of brain structures, including but not limited to only premotor areas (Kunst et al., 2019), the orange arrow from the cerebellum was drawn in Figure 4.1 to reach premotor circuits to highlight that its output effectively modifies the final motor output of the controller. It is possible that this modification is achieved through changing parameters in the upstream parts of the circuitry underlying the OMR and is mediated by other cerebellar outputs.

It is important to note, however, that the present study has several limitations that can be overcome in future studies. Although I believe that the cerebellum acts as a forward model that predicts expected feedback based on motor commands, alternative interpretations of the observed results are possible. Namely, the cerebellum may generate feedforward corrections of feedback motor commands, i.e. act as an inverse model in a feedback-error-learning scheme (Kawato, 1990, see Introduction section 1.1.2 for more details). A possible experiment that can disambiguate between these two cases will involve recordings from PCs during a long-term adaptation paradigm and comparing motor-related activity in the PCs before and after the adaptation. If PC activity constitutes the output of a forward model, one would expect less bout-related activity after the adaptation, as animals must have learnt to expect less feedback from a given motor command. If instead, the cerebellum learns an inverse transfer function, long-term adaptation to decreased reafference must elevate bout-related PC activity, as animals must have learnt that a stronger feedforward motor command is required to reach the desired state.

Another limitation is that the increase in bout kinematics during the ballistic period was observed not only after long-term adaptation to perturbed reafference but also in animals presented with normal reafference during the adaptation session (Figure 3.13). Although the normal reafference condition was calibrated to mimic the freely swimming condition as close as possible (Materials and methods sections 2.2 and 2.3.1), the visual feedback provided in the closed-loop assay to head-restrained larvae might still differ from what a freely swimming larvae normally receives. The reasons for this may include imperfectness and processing time of the velocity estimator and/or delays involved in updating the projected stimulus. This limitation is confounded by the lack of any vestibular feedback in head-restrained preparations. The mismatch between the natural visuo-vestibualar feedback and feedback provided in the closed-loop assay might underlie long-term changes in bout kinematics in normal reafference control animals. To test this, one could transfer the long-term adaptation experiments to a freely swimming condition, where sensory feedback that larvae receive is natural by definition. If in this case the ballistic kinematics of the swimming bouts would change only after long-term adaptation to perturbed visual feedback, this will prove that long-term adaptation of this behavioral parameter is indeed driven by a novel reafference condition.

Nevertheless, the present study demonstrates that the cerebellum is involved in long-term adaptation of locomotion in larval zebrafish, but not in acute online behavioral corrections in response to perturbed reafference. Given the advantages of larval zebrafish as a model system for experimental research, this provides an exciting opportunity for future investigations on cerebellar internal models and their role in adaptive behaviors.

5. Appendix

5.1 List of abbreviations

CF	climbing fiber
CNS	central nervous system
DCN	deep cerebellar nuclei
DRN	dorsal raphe nucleus
dpf	days post-fertilization
EC	eurydendroid cell
epNtr	enhanced nitroreductase
FMS	forward motion sensor
GC	granule cell
IO	inferior olive
IR	infrared
LED	light emitting diode
MF	mossy fiber
MI	motor integrator
MOG	motor output generator
MTZ	Metronidazole
Ntr	nitroreductase
OMR	optomotor response
OT	optic tectum
PC	Purkinje cell
PF	parallel fiber
preT	pretectum
RMS	reverse motion sensor
ROI	region of interest
SEM	standard error of mean
SI	sensory integrator
Thal	thalamus
TL	wild-type Tüpfel long-fin zebrafish strain
TMS	transcranial magnetic stimulation

5.2 List of tables and figures

Table 1. Zebrafish strains used in this thesis.. 27
Table 2. Numbers of animals tested in the behavioral experiments 37

Figure 1.1. Feedback controller 3
Figure 1.2. Possible placements of internal models within a feedback control system 7
Figure 1.3. Main connections of the olivo-cerebellar system 11
Figure 1.4. Olivo-cerebellar cells in the larval zebrafish brain 20
Figure 2.1. Closed-loop experimental assay and an example trial 31
Figure 2.2. Reafference conditions used in this thesis 34
Figure 2.3. Light sheet setup and imaged brain area 43
Figure 3.1. Acute OMR adaptation to gain of the closed loop 49
Figure 3.2. Acute OMR adaptation to lag of the reafference 51
Figure 3.3. Acute OMR adaptation to gain drop 53
Figure 3.4. Ballistic and reactive periods of swimming bouts 54
Figure 3.5. Acute adaptation of ballistic and reactive bout power 55
Figure 3.6. Targeted pharmaco-genetic ablation of PCs 57
Figure 3.7. Acute OMR adaptation after PC ablation 59
Figure 3.8. Feedback controller of acute adaptation 62
Figure 3.9. Acute adaptation of the feedback control model 63
Figure 3.10. Sensory and motor ROIs in the larval zebrafish brain 65
Figure 3.11. Sensory integration in the larval zebrafish brain 67
Figure 3.12. Changes in first bout duration during long-term OMR adaptation 69
Figure 3.13. Changes in first bout power during long-term OMR adaptation 70
Figure 3.14. Long-term OMR adaptation after PC ablation 72
Figure 4.1. Proposed mechanism of acute and long-term OMR adaptation 78

5.3 MATLAB code of the feedback control model of acute adaptation

The model should be operated using two main functions: *model_iteration* and *experiment_iteration* that are iteratively called in the parent program, in which the experimental protocol is defined. *Model_iteration* function computes the output of the model given its previous state, current sensory stimulus and a set of model parameters. *Experiment_iteration* function adds the reafference to the sensory stimulus given the output of the model, exafferent stimulus and reafference condition. Example below shows an experimental protocol used in Figure 3.8b, in which the grating was moving forward at 10 mm/s for 15 s, preceded and followed by 3-s periods of static grating. Reafference conditions were individually selected for each bout to illustrate that the output of the model depends on reafference in a way, similar to the real animals. The *experiment_iteration* and *model_iteration* functions are presented after the parent program.

```
%% define timing of the protocol
dt = 0.005; % sampling period of the modelled experiment, in seconds
mov_dur = 15; % duration of the moving grating, in seconds
stat_dur = 3; % duration of the static grating, in seconds
num_frames = round((mov_dur + 2 * stat_dur) / dt); % total number of
                                                    frames in the protocol
% define frame numbers, when the grating starts and stops moving:
gr_starts = round(stat_dur / dt);
gr_ends = round((stat_dur + mov_dur) / dt);
% define the initial grating speed array (in mm/s):
grspeed = zeros(1, num_frames);
grspeed(gr_starts:gr_ends) = 10;
% pre-allocate the output behavioral array of the modelled fish:
swim = false(1, num_frames);
%% define the reafference conditions used in the protocol
% define the reafference conditions for each bout (N = 7):
reaf = [1        0     0     0     0; ...
        0        0     0     0     0; ...
        0.33     0     0     0     0; ...
        1.66     0     0     0     0; ...
        1        0.15  0     0     0; ...
        1        0.15  1     0     0; ...
        1        0     0     0.15  0.3];
```

```
      % each row encodes reafference condition of one bout
      % each column represents one parameter of reafference condition:
      % reaf(:, 1) - gain of the closed loop
      % reaf(:, 2) - lag of the reafference, in seconds with respect to
                     the bout onset
      % reaf(:, 3) - is the lag shunted (1) or not (0)?
      % reaf(:, 4) - start of the gain drop period, in seconds with
                     respect to the bout onset
      % reaf(:, 5) - end of the gain drop period, in seconds with
                     respect to the bout onset
% therefore, the order of reafference conditions in this example trial is
% the same is in Figure 3.8b: normal reafference, open loop, 0.33 gain,
% 1.66 gain, 150 ms lag, 150 ms shunted lag, gain drop 1100

% define the reafference condition that will be used after the seventh
% bout, in case they appear (let it be the normal reafference):
reaf0 = [1 0 0 0 0];

% express the reafference parameters, that are expressed in seconds, in
% sampling frames, by dividing them by the sampling period:
reaf(:, 2) = round(reaf(:, 2) / dt);
reaf(:, 4) = round(reaf(:, 4) / dt);
reaf(:, 5) = round(reaf(:, 5) / dt);



%% define the parameters of the model
sens_delay = 0.22; % sensory processing delay, in seconds
sens_delay = round(sens_delay / dt); % now, expressed in frames
% set of eight parameters of the model:
par = [0.161, 0.15, 2.8, 2.5, 0.8, 0.9, 0.5, 0.52];
      % par(1) - weight between FMS and SI
      % par(2) - weight between RMS and SI
      % par(3) - time constant of SI, in seconds
      % par(4) - weight between MI and MOG
      % par(5) - weight of feed-forward self-excitation of motor output
      % par(6) - motor command threshold
      % par(7) - weight between motor output command and MI
      % par(8) - time constant of MI, in seconds

% express the time constants in sampling frames, by dividing the sampling
% period by the time constants. This is convinient because in the
% equasions of the leaky integrator time constants are denominators:
par(3) = dt / par_trial(3);
par(8) = dt / par_trial(8);

% pre-allocate the state of the model (see the description below):
model_state = zeros(5, num_frames);
```

```
%% run the protocol!
bout_counter = 0; % bout counter used to determine the current
                                                 reafference condition
% technical variables used to implement lags and gain drops:
fr_since_bout_start=0;
fr_since_bout_end=inf;
reaf=[reaf0; reaf]; % this is done because it is convinient to take the
                   n+1th reafference conditiom for the nth bout (see below)

% run a loop frame by frame:
for t = sens_delay + 1 : num_frames

    % determine current reafference condition:
    if bout_counter <= size(reaf, 1);
        this_reaf = reaf(bout_counter + 1, :);
    else
        this_reaf = reaf0;
    end

    % update the sensory stimulus grspeed(t) given the previous model's
    % output swim(t - 1) and reafference condition this_reaf
    [grspeed(t), fr_since_bout_start, fr_since_bout_end] = ...
      experiment_iteration (grspeed(t), swim(t - 1), ...
      fr_since_bout_start, fr_since_bout_end, this_reaf);

    % compute the current model's output swim(t) and state of the model
    % model_state(:, t) given its previous state model_state(:, t - 1)
    % and the sensory stimulus (given the sensory processing delay):
    [swim(t), model_state(:,t)] = model_iteration(swim(t - 1), ...
      model_state(:, t - 1), grspeed(t - sens_delay), par);
    % if a bout has just started, update the counter
    if swim(t)
        if ~swim(t - 1)
            bout_counter = bout_counter + 1;
        end
    end
end

% now one just needs to plot grspeed, model_state and swim to reproduce
% figure 3.8b
```

```
function [grspeed, fr_since_bout_start, fr_since_bout_end] = ...
experiment_iteration (grspeed, swim, fr_since_bout_start, ...
fr_since_bout_end, reaf)
%
% This function adds reafference to the exafferent stimulus grspeed given
% the output of the model swim and reafference condition reaf. See
% description of the input and output variables above.

% if the modelled fish swims, compute the reafferent sensory stimulus
% based on reafference condition
if swim
    fr_since_bout_start = fr_since_bout_start + 1;
    fr_since_bout_end = 0;
    if fr_since_bout_start > reaf(2) % if bout is longer than lag
        if fr_since_bout_start < reaf(4) || ...
            fr_since_bout_start > reaf(5) % and if gain is not dropped
            grspeed = grspeed - reaf(1) * 20; % then provide some
% reafference, depending on the gain. 20 is the velocity multiplication
% factor that ensures that at gain 1, the modelled fish swims at 20 mm/s
        end
    end
else
    fr_since_bout_end = fr_since_bout_end + 1;
    fr_since_bout_start = 0;
    if reaf(3) == 0 % if lag is not shunted
        if fr_since_bout_end <= reaf(2) % if bout is longer than lag
            grspeed = grspeed - reaf(1) * 20; % then provide reafference
        end
    end
end
% In all other cases, the updated grating speed will be the same as
% before, i.e. fish will receive no reafference
```

```
function [swim, model_state] = model_iteration(swim, model_state, ...
grspeed, par)

% This function computes the output of the model together with it’s next
% state, given the previous state, current stimulus and a set of
% parameters
%
% Inputs:
%
% 1. swim - a binary variable that tells if the modelled fish was
%           swimming before this iteration (1) or not (0)
%
% 2. model_state - previous state of the model
%       model_state(1) - activity of the forward motion sensor (FMS)
%       model_state(2) - activity of the reverse motion sensor (RMS)
%       model_state(3) - activity of the sensory integrator (SI)
%       model_state(4) - activity of the motor output generator (MOG)
%       model_state(5) - activity of the motor integrator (MI)
%
% 3. grspeed - current grating speed [mm/s]
%
% 4. par – set of eight parameters of the model
%       par(1) - weight between FMS and SI
%       par(2) - weight between RMS and SI
%       par(3) – sampling period (dt) divided by time constant of SI
%       par(4) - weight between MI and MOG
%       par(5) - weight of feed-forward self-excitation of motor output
%       par(6) – motor command threshold
%       par(7) - weight between motor output command and MI
%       par(8) – sampling period (dt) divided by time constant of MI
%
% Outputs:
%
% 1. swim - a binary variable that tells if the modelled fish will swim
%           after this iteration (1) or not (0)
%
% 2. model_state - state of the model after this iteration
% compute activity of FMS (positively rectified grating speed)
model_state(1) = max(grspeed, 0);

% compute activity of RMS (negatively rectified grating speed)
model_state(2) = - min(grspeed, 0);

% compute activity of SI (positively rectified leaky integrator with
saturation at 1)
model_state(3) = par(3) * par(1) * model_state(1) - par(3) * par(2) * ...
                  model_state(2) - (par(3) - 1) * model_state(3),1),0);
model_state(3) = max(min(model_state(3), 1), 0);
% compute activity of MOG (positively rectified, activated by SI and
inhibited by MI)
model_state(4) = model_state(3) - par(4) * model_state(5);
model_state(4) = max(model_state(4), 0);

% compute motor output (fish swims if activity of MOG + self-excitation
is greater than the motor command threshold)
swim = model_state(4) + par(5) * swim > par(6);

% activity of MI (leaky integrator with saturation at 1)
model_state(5) = par(8) * par(7) * swim - (par(8) - 1) * model_state(5);
model_state(5) = min(model_state(5), 1);
```

Bibliography

Ahrens, M. B., Li, J. M., Orger, M. B., Robson, D. N., Schier, A. F., Engert, F. and Portugues, R. (2012). Brain-wide neuronal dynamics during motor adaptation in zebrafish. *Nature* 485, 471–477.

Aizenberg, M. and Schuman, E. M. (2011). Cerebellar-dependent learning in larval zebrafish. *J. Neurosci.* 31, 8708–8712.

Albus, J. S. (1971). A theory of cerebellar function. *Math. Biosci.* 10, 25–61.

Bahl A., Engert F. (2019). Neural circuits for evidence accumulation and decision-making in larval zebrafish. *Nat. Neurosci.* (in press).

Barlow, H. B. and Hill, R. M. (1963). Selective Sensitivity to Direction of Movement in Ganglion Cells of the Rabbit Retina. *Science* 139, 412–414.

Barlow, H. B., Hill, R. M. and Levick, W. R. (1964). Retinal ganglion cells responding selectively to direction and speed of image motion in the rabbit. *J. Physiol.* 173, 377–407.

Barnett-Cowan, M. and Harris, L. R. (2009). Perceived timing of vestibular stimulation relative to touch, light and sound. *Exp. brain Res.* 198, 221–231.

Borla, M. A., Palecek, B., Budick, S. and O'Malley, D. M. (2002). Prey capture by larval zebrafish: evidence for fine axial motor control. *Brain. Behav. Evol.* 60, 207–229.

Brenner, E. and Smeets, J. B. J. (2003). Fast corrections of movements with a computer mouse. *Spat. Vis.* 16, 365–376.

Budick, S. A. and O'Malley, D. M. (2000). Locomotor repertoire of the larval zebrafish: swimming, turning and prey capture. *J. Exp. Biol.* 203, 2565–2579.

Burgess, H. A. and Granato, M. (2007). Modulation of locomotor activity in larval zebrafish during light adaptation. *J. Exp. Biol.* 210, 2526–2539.

Burrill, J. D. and Easter, S. S. (1994). Development of the retinofugal projections in the embryonic and larval zebrafish (Brachydanio rerio). *J. Comp. Neurol.* 346, 583–600.

Chen, T. W., Wardill, T. J., Sun, Y., Pulver, S. R., Renninger, S. L., Baohan, A., Schreiter, E. R., Kerr, R. A., Orger, M. B., Jayaraman, V., et al. (2013). Ultrasensitive fluorescent proteins for imaging neuronal activity. *Nature* 499, 295–300.

Curado, S., Anderson, R. M., Jungblut, B., Mumm, J., Schroeter, E. and Stainier, D. Y. R. (2007). Conditional Targeted Cell Ablation in Zebrafish : A New Tool for Regeneration Studies. *Dev. Dynam*. 236, 1025–1035.

de Zeeuw, C. I., Holstege, J. C., Ruigrok, T. J. and Voogd, J. (1989). Ultrastructural study of the GABAergic, cerebellar, and mesodiencephalic innervation of the cat medial accessory olive: anterograde tracing combined with immunocytochemistry. *J. Comp. Neurol.* 284, 12–35.

de Zeeuw, C. I., Hansel, C., Bian, F., Koekkoek, S. K. E., van Alphen, A. M., Linden, D. J. and Oberdick, J. (1998). Expression of a Protein Kinase C Inhibitor in Purkinje Cells Blocks Cerebellar LTD and Adaptation of the Vestibulo-Ocular Reflex. *Neuron* 20, 495–508.

Desmurget and Grafton (2000). Forward modeling allows feedback control for fast reaching movements. *Trends Cogn. Sci.* 4, 423–431.

Dietrich, H. and Straka, H. (2016). Prolonged vestibular stimulation induces homeostatic plasticity of the vestibulo-ocular reflex in larval Xenopus laevis. *Eur. J. Neurosci.* 44, 1787–1796.

Dow, R. S. (1942). The evolution and anatomy of the cerebellum. *Biol. Rev.* 17, 179–220.

Dragomir, E. I., Štih, V., Portugues, R. (2019). Evidence accumulation during a sensorimotor decision task revealed by whole-brain imaging. *Nat. Neurosci.* (in press).

Easter, S. S. and Nicola, G. N. (1997). The development of eye movements in the zebrafish (Danio rerio). *Dev. Psychobiol.* 31, 267–76.

Eccles, J. C., Llinás, R. and Sasaki, K. (1966). The excitatory synaptic action of climbing fibres on the Purkinje cells of the cerebellum. *J. Physiol.* 182, 268–96.

Flanagan, J. R. and Tresilian, J. R. (1994). Grip-load force coupling: a general control strategy for transporting objects. *J. Exp. Psychol. Hum. Percept. Perform.* 20, 944–957.

Flanagan, J. R. and Wing, A. (1990). The stability of precision grip forces during cyclic arm movements with a hand-held load. *Exp. Brain Res.* 105, 455–464.

Flanagan, J. R. and Wing, A. (1993). Modulation of grip force with load force during point-to-point arm movements. *Exp. Brain Res.* 95, 131–143.

Flanagan, J. R. and Wing, A. M. (1997). The role of internal models in motion planning and control: evidence from grip force adjustments during movements of hand-held loads. *J. Neurosci.* 17, 1519–1528.

Flanagan, J. R., Tresilian, J. and Wing, A. M. (1993). Coupling of grip force and load force during arm movements with grasped objects. *Neurosci. Lett.* 152, 53–56.

Flanagan, J. R., Vetter, P., Johansson, R. S. and Wolpert, D. M. (2003). Prediction precedes control in motor learning. *Curr. Biol.* 13, 146–150.

Flanders, M. and Cordo, P. J. (1989). Kinesthetic and visual control of a bimanual task: specification of direction and amplitude. *J. Neurosci.* 9, 447–453.

Flanders, M., Cordo, P. J. and Anson, J. G. (1986). Interaction between visually and kinesthetically triggered voluntary responses. *J. Mot. Behav.* 18, 427–448.

Fredette, B. J. and Mugnaini, E. (1991). The GABAergic cerebello-olivary projection in the rat. *Anat. Embryol. (Berl).* 184, 225–243.

Gabriel, J. P., Trivedi, C. A., Maurer, C. M., Ryu, S. and Bollmann, J. H. (2012). Layer-specific targeting of direction-selective neurons in the zebrafish optic tectum. *Neuron* 76, 1147–1160.

Gamlin, P. D. R. (2006). The pretectum: connections and oculomotor-related roles. *Prog. Brain Res.* 151, 379–405.

Harmon, T. C., Magaram, U., McLean, D. L. and Raman, I. M. (2017). Distinct responses of Purkinje neurons and roles of simple spikes during associative motor learning in larval zebrafish. *Elife* 6.

Hinz, F. I., Aizenberg, M., Tushev, G. and Schuman, E. M. (2013). Protein synthesis-dependent associative long-term memory in larval zebrafish. *J. Neurosci.* 33, 15382–15387.

Ikenaga, T., Yoshida, M. and Uematsu, K. (2006). Cerebellar efferent neurons in teleost fish. *Cerebellum* 5, 268–274.

Imamizu, H., Miyauchi, S., Tamada, T., Sasaki, Y., Takino, R., Pütz, B., Yoshioka, T. and Kawato, M. (2000). Human cerebellar activity reflecting an acquired internal model of a new tool. *Nature* 403, 192–195.

Imamizu, H., Kuroda, T., Miyauchi, S., Yoshioka, T. and Kawato, M. (2003). Modular organization of internal models of tools in the human cerebellum. *Proc. Natl. Acad. Sci. U. S. A.* 100, 5461–5466.

Ito, M. (1982). Cerebellar control of the vestibulo-ocular reflex – around the flocculus hypothesis. *Annu. Rev. Neurosci.* 5, 275–96.

Ito, M., Sakurai, M. and Tongroach, P. (1982). Climbing fibre induced depression of both mossy fibre responsiveness and glutamate sensitivity of cerebellar Purkinje cells. *J. Physiol.* 324, 113–134.

Izawa, J., Criscimagna-Hemminger, S. E. and Shadmehr, R. (2012). Cerebellar contributions to reach adaptation and learning sensory consequences of action. *J. Neurosci.* 32, 4230–4239.

Kakei, S., Lee, J., Mitoma, H., Tanaka, H., Manto, M. and Hampe, C. S. (2019). Contribution of the Cerebellum to Predictive Motor Control and Its Evaluation in Ataxic Patients. *Front. Hum. Neurosci.* 13.

Kawato, M. (1990). Feedback-Error-Learning Neural Network for Supervised Motor Learning. In *Advanced Neural Computers*, pp. 365–372. Elsevier.

Kawato, M. (1999). Internal models for motor control and trajectory planning. *Curr. Opin. Neurobiol.* 9, 718–727.

Kawato, M. and Gomi, H. (1992a). The cerebellum and VOR/OKR learning models. *Trends Neurosci.* 15, 445–453.

Kawato, M. and Gomi, H. (1992b). A computational model of four regions of the cerebellum based on feedback-error learning. *Biol. Cybern.* 68, 95–103.

Kawato, M., Furukawa, K. and Suzuki, R. (1987). A hierarchical neural-network model for control and learning of voluntary movement. *Biol. Cybern.* 57, 169–185.

Kim, D. H., Kim, J., Marques, J. C., Grama, A., Hildebrand, D. G. C., Gu, W., Li, J. M. and Robson, D. N. (2017). Pan-neuronal calcium imaging with cellular resolution in freely swimming zebrafish. *Nat. Methods* 14, 1107–1114.

Kist, A. M., Knogler, L. D., Markov, D. A., Yildizoglu, T. and Portugues, R. (2017). Whole-Brain Imaging Using Genetically Encoded Activity Sensors in Vertebrates. In *Decoding Neural Circuit Structure and Function: Cellular Dissection Using Genetic Model Organisms* (ed. Çelik, A. and Wernet, M. F.), pp. 321–341. Cham: Springer International Publishing.

Knogler, L. D., Markov, D. A., Dragomir, E. I., Štih, V. and Portugues, R. (2017). Sensorimotor Representations in Cerebellar Granule Cells in Larval Zebrafish Are Dense, Spatially Organized, and Non-temporally Patterned. *Curr. Biol.* 27, 1288–1302.

Knogler, L. D., Kist, A. M. and Portugues, R. (2019). Motor context dominates output from purkinje cell functional regions during reflexive visuomotor behaviours. *Elife* 8.

Kubo, F., Hablitzel, B., Dal Maschio, M., Driever, W., Baier, H. and Arrenberg, A. B. (2014). Functional architecture of an optic flow-responsive area that drives horizontal eye movements in zebrafish. *Neuron* 81, 1344–1359.

Kunst, M., Laurell, E., Mokayes, N., Kramer, A., Kubo, F., Fernandes, A. M., Förster, D., Dal Maschio, M. and Baier, H. (2019). A Cellular-Resolution Atlas of the Larval Zebrafish Brain. *Neuron* 103, 21-38.e5.

Li, J. M. (2012). Identification of an operant learning circuit by whole brain functional imaging in larval zebrafish. Doctoral dissertation, Harvard University.

Lisberger, S. G. (2009). Internal models of eye movement in the floccular complex of the monkey cerebellum. *Neuroscience* 162, 763–776.

Lister, J. A., Robertson, C. P., Lepage, T., Johnson, S. L. and Raible, D. W. (1999). Nacre encodes a zebrafish microphthalmia-related protein that regulates neural-crest-derived pigment cell fate. *Development* 126, 3757–3767.

Llinás, R. R., Walton, K. D. and Lang, E. J. (2004). Cerebellum. In *The synaptic organisation of the brain* (ed. Shepherd, G. M.), pp. 271–309. New York: Oxford University Press.

Marr, D. (1969). A theory of cerebellar cortex. *J. Physiol.* 202, 437–470.

Matsui, H., Namikawa, K., Babaryka, A. and Köster, R. W. (2014). Functional regionalization of the teleost cerebellum analyzed in vivo. *Proc. Natl. Acad. Sci. U. S. A.* 111, 11846–11851.

McElligott, M. B. and O'malley, D. M. (2005). Prey tracking by larval zebrafish: axial kinematics and visual control. *Brain. Behav. Evol.* 66, 177–196.

Miall, R. C., Christensen, L. O. D., Cain, O. and Stanley, J. (2007). Disruption of state estimation in the human lateral cerebellum. *PLoS Biol.* 5, e316.

Mischiati, M., Lin, H.-T., Herold, P., Imler, E., Olberg, R. and Leonardo, A. (2015). Internal models direct dragonfly interception steering. *Nature* 517, 333–338.

Naumann, E. A., Fitzgerald, J. E., Dunn, T. W., Rihel, J., Sompolinsky, H. and Engert, F. (2016). From Whole-Brain Data to Functional Circuit Models: The Zebrafish Optomotor Response. *Cell* 167, 947-960.e20.

Neuhauss, S. C., Biehlmaier, O., Seeliger, M. W., Das, T., Kohler, K., Harris, W. A. and Baier, H. (1999). Genetic disorders of vision revealed by a behavioral screen of 400 essential loci in zebrafish. *J. Neurosci.* 19, 8603–8615.

Nikolaou, N., Lowe, A. S., Walker, A. S., Abbas, F., Hunter, P. R., Thompson, I. D. and Meyer, M. P. (2012). Parametric Functional Maps of Visual Inputs to the Tectum. *Neuron* 76, 317–324.

Nowak, D. A., Topka, H., Timmann, D., Boecker, H. and Hermsdörfer, J. (2007). The role of the cerebellum for predictive control of grasping. *Cerebellum* 6, 7–17.

Oteiza, P., Odstrcil, I., Lauder, G., Portugues, R. and Engert, F. (2017). A novel mechanism for mechanosensory-based rheotaxis in larval zebrafish. *Nature* 547, 445–448.

Pisharath, H., Rhee, J. M., Swanson, M. A., Leach, S. D. and Parsons, M. J. (2007). Targeted ablation of beta cells in the embryonic zebrafish pancreas using E. coli nitroreductase. *Mech. Dev.* 124, 218–229.

Portugues, R. and Engert, F. (2011). Adaptive locomotor behavior in larval zebrafish. *Front. Syst. Neurosci.* 5.

Portugues, R., Feierstein, C. E., Engert, F. and Orger, M. B. (2014). Whole-brain activity maps reveal stereotyped, distributed networks for visuomotor behavior. *Neuron* 81, 1328–1343.

Purves, D., Augustine, G. J., Fitzpatrick, D., Hall, W. C., LaMantia, A.-S., McNamara, J. O. and Williams, S. M. (2004). *Neuroscience*. 3d edition. Sunderland: Sinauer Associates.

Randlett, O., Wee, C. L., Naumann, E. A., Nnaemeka, O., Schoppik, D., Fitzgerald, J. E., Portugues, R., Lacoste, A. M. B., Riegler, C., Engert, F., et al. (2015). Whole-brain activity mapping onto a zebrafish brain atlas. *Nat. Methods* 12, 1039–1046. Link to the Z-Brain atlas: https://engertlab.fas.harvard.edu/Z-Brain.

Raymond, J. L., Lisberger, S. G. and Mauk, M. D. (1996). The cerebellum: a neuronal learning machine? *Science* 272, 1126–1131.

Rohlfing, T. and Maurer, C. R. (2003). Nonrigid image registration in shared-memory multiprocessor environments with application to brains, breasts, and bees. *IEEE Trans. Inf. Technol. Biomed.* 7, 16–25.

Sabes, P. N. (2000). The planning and control of reaching movements. *Curr. Opin. Neurobiol.* 10, 740–746.

Saunders, J. A. and Knill, D. C. (2003). Humans use continuous visual feedback from the hand to control fast reaching movements. *Exp. brain Res.* 152, 341–352.

Saunders, J. A. and Knill, D. C. (2005). Humans use continuous visual feedback from the hand to control both the direction and distance of pointing movements. *Exp. brain Res.* 162, 458–473.

Schindelin, J., Arganda-Carreras, I., Frise, E., Kaynig, V., Longair, M., Pietzsch, T., Preibisch, S., Rueden, C., Saalfeld, S., Schmid, B., et al. (2012). Fiji: An open-source platform for biological-image analysis. *Nat. Methods* 9, 676–682.

Severi, K. E., Portugues, R., Marques, J. C., O'Malley, D. M., Orger, M. B. and Engert, F. (2014). Neural Control and Modulation of Swimming Speed in the Larval Zebrafish. *Neuron* 83, 692–707.

Shadmehr, R., Smith, M. A. and Krakauer, J. W. (2010). Error correction, sensory prediction, and adaptation in motor control. *Annu. Rev. Neurosci.* 33, 89–108.

Shidara, M., Kawano, K., Gomi, H. and Kawato, M. (1993). Inverse-dynamics model eye movement control by Purkinje cells in the cerebellum. *Nature* 365, 50–52.

Shinoda, Y., Sugiuchi, Y., Futami, T. and Izawa, R. (1992). Axon collaterals of mossy fibers from the pontine nucleus in the cerebellar dentate nucleus. *J. Neurophysiol.* 67, 547–560.

Sotelo, C. (2008). Viewing the cerebellum through the eyes of Ramón Y Cajal. *Cerebellum* 7, 517–522.

Starr, A., McKeon, B., Skuse, N. and Burke, D. (1981). Cerebral potentials evoked by muscle stretch in man. *Brain* 104, 149–166.

Štih, V., Petrucco, L., Kist, A. M. and Portugues, R. (2019). Stytra: An open-source, integrated system for stimulation, tracking and closed-loop behavioral experiments. PLoS Comput. Biol. 15. Link to Stytra: https://github.com/portugueslab/stytra.

Tabata, T. and Kano, M. (2009). Synaptic Plasticity in the Cerebellum. In *Handbook of Neurochemistry and Molecular Neurobiology* (ed. Lajtha, A. and Mikoshiba, K.), pp. 63–86. Boston: Springer US.

Tabor, K. M., Bergeron, S. A., Horstick, E. J., Jordan, D. C., Aho, V., Porkka-Heiskanen, T., Haspel, G. and Burgess, H. A. (2014). Direct activation of the Mauthner cell by electric field pulses drives ultrarapid escape responses. *J. Neurophysiol.* 112, 834–844.

Takeuchi, M., Matsuda, K., Yamaguchi, S., Asakawa, K., Miyasaka, N., Lal, P., Yoshihara, Y., Koga, A., Kawakami, K., Shimizu, T., et al. (2015). Establishment of Gal4 transgenic zebrafish lines for analysis of development of cerebellar neural circuitry. *Dev. Biol.* 397, 1–17.

Turner, L., Ryu, W. S. and Berg, H. C. (2000). Real-time imaging of fluorescent flagellar filaments. *J. Bacteriol.* 182, 2793–2801.

Wolf, S., Dubreuil, A. M., Bertoni, T., Böhm, U. L., Bormuth, V., Candelier, R., Karpenko, S., Hildebrand, D. G. C., Bianco, I. H., Monasson, R., et al. (2017). Sensorimotor computation underlying phototaxis in zebrafish. *Nat. Commun.* 8.

Wolpert, D. M. and Kawato, M. (1998). Multiple paired forward and inverse models for motor control. *Neural Netw.* 11, 1317–1329.

Wolpert, D., Ghahramani, Z. and Jordan, M. (1995). An internal model for sensorimotor integration. *Science* 269, 1880–1882.

Wolpert, D. M., Miall, R. C. and Kawato, M. (1998). Internal models in the cerebellum. *Trends Cogn. Sci.* 2, 338–347.

Yavari, F., Mahdavi, S., Towhidkhah, F., Ahmadi-Pajouh, M.-A., Ekhtiari, H. and Darainy, M. (2016). Cerebellum as a forward but not inverse model in visuomotor adaptation task: a tDCS-based and modeling study. *Exp. brain Res.* 234, 997–1012.

Yuan, J., Fahrner, K. A., Turner, L. and Berg, H. C. (2010). Asymmetry in the clockwise and counterclockwise rotation of the bacterial flagellar motor. *Proc. Natl. Acad. Sci. U. S. A.* 107, 12846–12849.

Declaration of contributions

Daniil A. Markov and Ruben Portugues conceived the study. Daniil A. Markov performed experiments, analyzed the data, developed the model, and wrote the thesis. Andreas Kist generated the *PC*:epNtr-tagRFP transgenic line and developed the gain drop paradigm. Luigi Petrucco programmed the experimental protocols, helped with the functional imaging experiments and pre-processed the raw light sheet data.

List of publications

Markov, D. A., Kist, A. M., Petrucco, L. and Portugues R. Purkinje cells modify a feedback controller involved in locomotion of larval zebrafish. *In preparation for submission.*

Valera, G.*****, Markov, D. A.*****, Bijari, K., Randlett, O., Argharsharghi, A., Baudoin, J.-P., Ascoli, G. A., Portugues, R. and López-Schier, H. A neuronal blueprint for directional mechanosensation in larval zebrafish. *In preparation for resubmission*.

***** equal-contributing authors

Kist, A. M., Knogler, L. D., Markov, D. A., Yildizoglu, T. and Portugues, R. (2017). Whole-Brain Imaging Using Genetically Encoded Activity Sensors in Vertebrates. In *Decoding Neural Circuit Structure and Function: Cellular Dissection Using Genetic Model Organisms* (ed. Çelik, A. and Wernet, M. F.), pp. 321–341. Cham: Springer International Publishing.

Knogler, L. D., Markov, D. A., Dragomir, E. I., Štih, V. and Portugues, R. (2017). Sensorimotor Representations in Cerebellar Granule Cells in Larval Zebrafish Are Dense, Spatially Organized, and Non-temporally Patterned. *Curr. Biol.* 27, 1288–1302.

Curriculum vitae

Education

Sep 2014 – Aug 2020	Ph.D. candidate at Max Planck Institute of Neurobiology, Sensorimotor Control Lab (Munich, Germany) Ph.D. program: IMPRS-LS (International Max Planck Research School for Molecular Life Sciences: From Biological Structures to Neural Circuits) University: Ludwig Maximilian University of Munich, Faculty of Biology (2015 – 2018)
Sep 2009 – Jun 2014	Undergraduate student at Lomonosov Moscow State University, Faculty of Biology, Department of Higher Nervous Activity (Moscow, Russia) Obtained degree: Specialist in Physiology (Diploma with Honors)

Research Experience

Sep 2014 – Aug 2020	Ph.D. candidate at Max Planck Institute of Neurobiology, Sensorimotor Control Lab (Munich, Germany) PhD project: Involvement of cerebellar Purkinje cells in adaptive locomotion of larval zebrafish PhD Supervisor: Dr. Ruben Portugues
Sep 2012 – Jun 2014	Research assistant at Institute of Higher Nervous Activity and Neurophysiology of Russian Academy of Science, Lab of Functional Biochemistry of the Nervous System (Moscow, Russia) Diploma project: Olfactory bulbectomy impact on the state of forebrain cholinergic system Course project 2: The study of nootropic effect of derivatives of pantothenic acid Course project 1: Experimental approaches to study stress in animals Supervisor: Dr. Michael Y. Stepanichev

Work and Volunteer Experience

Jun 2018	Teaching assistant at TENSS (Transylvanian Experimental Neuroscience Summer School) (Sacalaia, Romania)	
Mar – May 2018	Scientific editor at Foundation for the Development of Culture and Education "Moscow Time" (Moscow, Russia)	
	Duty:	Scientific editing of Russian translation of the book by Robert Sapolsky “Behave: The Biology of Humans at Our Best and Worst”

Honors and Awards

Sep 2014 – present	IMPRS-LS Ph.D. fellowship (Munich, Germany)
Feb 2014	Presidential prize for talented young people (Moscow, Russia)

Presentations

Nov 2018	SfN Neuroscience Meeting (San Diego, USA)	
	Poster presentation:	Sensory and Motor Representations in the Inferior Olive
Jul 2018	FENS Forum of Neuroscience (Berlin, Germany)	
	Poster presentation:	Sensory and Motor Representations in the Inferior Olive